Arabian Journal of Geosciences (2018) 11: 369
https://doi.org/10.1007/s12517-018-3701-5

ORIGINAL PAPER

Active tectonics analysis of the Kalmard fault zone, Central Iran

M. Moumeni-Taromsari[1] · M. Dehbozorgi[1] · R. Nozaem[2] · A. Yassaghi[3]

Received: 4 August 2017 / Accepted: 18 June 2018 / Published online: 10 July 2018

Abstract
Central-East Iran has numerous active Quaternary faults. This paper focuses on the analysis of geomorphic and structural characteristics of the Kalmard fault zone, including major NE–SW striking fault segments that cuts across the basement and the sedimentary cover in the Ozbak-Kuh area of Central-East Iran. Because of the absence of definite earthquakes through the Kalmard fault zone in contrast to other parts of Central Iran, we used morphotectonic methods in combination of structural studies to evaluate active tectonics of this area. Detailed structural assessment of satellite images and analysis of geomorphic indices, together with field surveys allowed us to evaluate the recent tectonic activity and support a Quaternary age for it. We used six morphometric indices including the stream-gradient index (SL), drainage basin asymmetry (Af), hypsometric integral (Hi), valley floor width–valley height ratio (Vf), drainage basin shape (Bs), and mountain-front sinuosity (Smf). We combined these indices to yield the relative active tectonics index (Iat). Based on Iat values, the study area includes class 1 (very high activity), class 2 (high), class 3 (moderate), and class 4 (low). Also the normalized steepness index (Ksn) represents a significant pattern of high values in the eastern and southeastern parts of the study area which correspond with high values of Iat index. The output is consistent with both landforms and structures observed during the field work. In particular, the high relative tectonic activity (classes 1 and 2) largely corresponds to F1 (the eastern segment of the Kalmard Fault Zone) in the Ozbak-Kuh area, while the moderate class of tectonic activity caracterizes F2 (the western segment of the Kalmarad Fault Zone). The older geological structures in the middle part of the area show the lowest relative tectonic activity. The results of this study indicate that the Kalmard fault zone is one of the major Quaternary fault zones of Central-East Iran which is potentially active.

Keywords Active tectonics · Geomorphic indices · Kalmard fault zone, Ozbak-Kuh · Central-East Iran

Introduction

Rising mountains are different from tectonically inactive landscapes. We should scrutinize landforms and the geomorphic processes that create them in order to recognize if they are still active (Bull 2009). The landforms of the eastern part of Central Iran like straight mountain fronts, deformed Quaternary deposits, fault scarps, and triangular facets represent recent tectonic activity. The Cenozoic deformation in Iran is the result of the Arabia–Eurasia convergence that culminated with the Arabia–Eurasia collision at the Eocene–Oligocene boundary (Agard et al. 2011; Allen et al. 2004; Mouthereau et al. 2012). GPS vectors indicate a current NNE motion of the Arabian plate relative to Eurasia of 22 ± 2 mm year^{-1} (Vernant et al. 2004).

The Kalmard fault zone is considered as one of the major fault zones of Central Iran (Berberian and Mohajer-Ashjai 1977) (Fig. 1), which activity that led to the growth of the Ozbak-Kuh Mountains. The absence of definite earthquakes through the Kalmard fault zone in contrast to other parts of Central Iran, however limits the possibility of seismological evaluation of its current tectonic activity.

✉ M. Dehbozorgi
m_dehbozorgi@khu.ac.ir

M. Moumeni-Taromsari
mohammad.moumeni@gmail.com; std_moumeni@khu.ac.ir

R. Nozaem
nozaem@ut.ac.ir

A. Yassaghi
yassaghi@modares.ac.ir

[1] Department of Earth Sciences, Kharazmi University, Tehran, Iran

[2] School of Geology, College of Science, University of Tehran, Tehran, Iran

[3] Faculty of Science, Tarbiat Modares University, Tehran, Iran

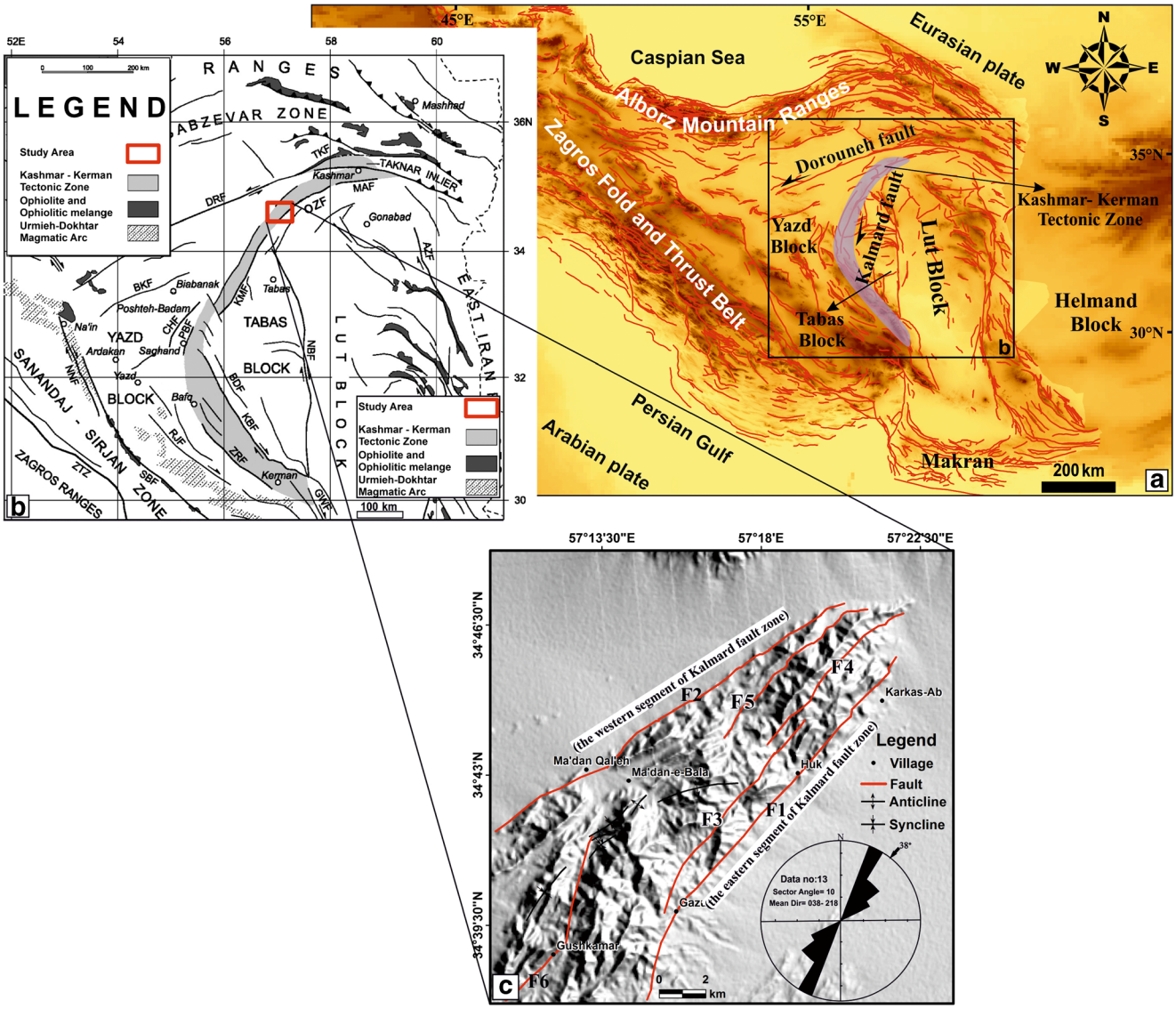

Fig. 1 Location of the study area in the Central Iran, (**a**) topographic map, blocks and faults of Iran and the middle east, (**b**) the structural map of Central East Iran and its crustal blocks (compiled from Berberian and King, 1981; Jackson and McKenzie 1984; Lindenberg et al., 1984; Haghipour and Aghanabati 1989; Alavi 1991). AZF = Abiz Fault; BDF = Behabad Fault, BKF = Biabanak Fault, CHF = Chapedony Fault, DRF = Doruneh Fault, GWF = Gowk Fault, KBF = Kuhbanan Fault, MAF = Mehdiabad Fault, MBF = Minab Fault, NAF = Nostratabad Fault, NHF = Nehbandan Fault, NNF = Na'in Fault, RJF = Rafsanjan Fault, SBF = Shahre-Babak Fault, TKF = Taknar Fault, KFZ = Kalmard Fault zone, ZRF = Zarand Fault, and ZTZ = Zagros Thrust Zone. Modification Panel (**b**) is after Ramezani and Tucker 2003. C) Hillshade image, structural map and faults rose diagram of Ozbak-Kuh area

Thus, geomorphological studies are important to evaluate earthquake hazards in tectonically active areas where the seismological record is absent (Keller and Pinter 2002). In this study, we are using morphometric indicators to evaluate the recent activity of the Kalmard fault zone and its impact on the adjacent Ozbak-Kuh Mountains which is placed at the north western part of Lut block, where Quaternary faulting has been recently documented (Nozaem et al. 2013; Calzolari et al. 2015, 2016). We carried out a structural and morphotectonic analysis to examine the involvement of Quaternary deposits during faulting.

Geological and tectonic setting

The Ozbak-Kuh Mountains is a NNE–SSW oriented mountain range located in the Central Iran (Fig. 1), north of the Tabas Block that has been affected by faulting along the Kalmard fault zone, a major Quaternary Fault of Central Eastern Iran (Berberian and Mohajer-Ashjai 1977). Central Eastern Iran (also known as Central Iran Micro Continent) constitutes a mosaic of continental microblocks (Lut, Tabas, and Yazd) (Fig. 1) assembled along the Southern Eurasian margin during the long-lasting convergence history between Eurasia and various Gondwanian fragments (Alavi 1991;

Bagheri and Stampli 2008; Berberian and King 1981; Davoudzadeh et al. 1981; Ramezani and Tucker 2003; Stöcklin 1968; Takin 1972). Major strike–slip fault zones bind these tectonic blocks and have peculiar stratigraphy, deformation style, and pattern of recent seismicity (Berberian and King 1981). A nearly 600 km long, arcuate and structurally complex fault-bounded belt known as the Kashmar–Kerman Tectonic Zone, where Neoproterozoic and lower Paleozoic rocks are exposed (Ramezani and Tucker 2003), separates the Tabas and Yazd blocks. The main characteristic of the Central Eastern Iran is the occurrence of prominent active fault zones like the Kalmard fault. This fault strand, has a length of 250 km, and is considered a major transpressional fault of the Kashmar–Kerman tectonic zone (Berberian and Mohajer-Ashjai 1977). The main rock units of the Ozbak-Kuh Mountain are early to late Paleozoic limestone, sandstone, and shale known as the Lalun, Niur, Padeha and Baharam formations, respectivelly. Locally, in some parts of the Ozbak-Kuh Mountains, Tertiary and Quaternary conglomerates, evaporites and sandstones are exposed.

Methodology

Morphometric indices are helpful in active tectonics studies as they provide a quick assessment of vast regions. Using multiple morphotectonic indices, we can evaluate a relative tectonic activity for the study area. These indices are known to be useful in active tectonics studies (Bull and McFadden 1977; Keller and Pinter, 2002). We categorized the level of rock resistance shown in Fig. 2a based on rock types and field observations: very low (alluvial deposits), low (older alluvial fan deposit and weakly cemented Neogene Conglomerates), moderate (shale, marl and gypsum), high (limestone, sandstone, dolomite, and well cemented conglomerate) and very high (diabase and associated rocks). In this article, we computed six geomorphic indices: the stream length gradient (SL), drainage basin asymmetry (Af), hypsometric integral (Hi), ratio of valley floor width to valley height (Vf), drainage basin shape (Bs), and mountain-front sinuosity (Smf). We, then, calculated a single index (Iat) from the six indices to characterize the relative degree of tectonic activity.

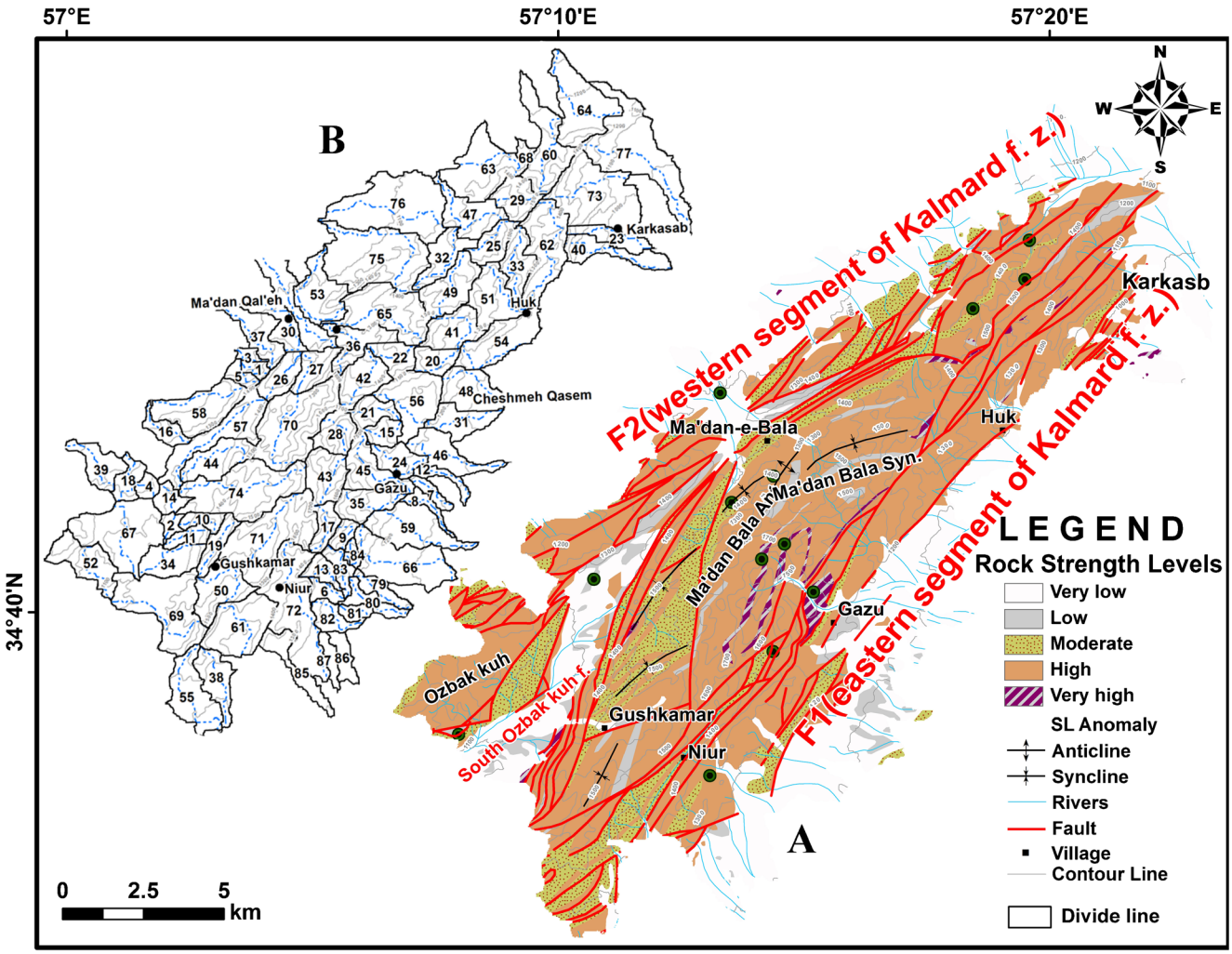

Fig. 2 (**a**) Distribution of rock strength levels and SL index anomalies, (**b**) Eighty-seven catchments in the study area

Furthermore, Normalized steepness index (Ksn) has been used to show the effect of the main faults on the rivers and also to compare with the Iat index values. Finally, for assessing the outcome of all indices and completing the result of this study, we performed fieldwork and compared field data with our morphometric analyses.

Morphometric analysis and indices

Morphometric indices

Morphometric indices are useful for studying areas experiencing tectonic deformation (Keller and Pinter 2002). In this study, we computed six geomorphic indices for every subbasin. Categorization of the result values for each catchment was into three classes, and then we summed and averaged these indices and ordered them into three classes of relative tectonic activity in the study area (El Hamdouni et al. 2008). We computed from digitized 1:25000 topographic maps and 30-m-resolution Digital Elevation Model of the study area. Subdivision of the study area is into 87 subbasins (Fig. 2b).

Stream length gradient index

Many processes shape the surface of planet Earth, but the action of running water is responsible for most subaerial landscapes. Uplift steepens stream gradients, which accelerates drainage basin erosion by making hill slopes steeper (Bull 2007). The SL index is one of the morphometric indices that indicate relationship between erosion and river flow procesess and this index correlates to stream authority (Hack 1973). Because the SL index is susceptible to variation in channel slope, it is an effective instrument for assessing river channels (Troiani and Della Seta 2008). The subsequent formula computes the SL equation (Hack 1973)

$$SL = (\Delta H/\Delta Lr)\ Lsc, \text{where} \quad (1)$$

ΔH is change in elevation, ΔLr indicates the length of the reach between two adjacent contour lines, and Lsc is the total channel length from the divide to the midpoint of the reach; moreover, the SL index can be employed to appraise relative tectonic activity (Keller and Pinter 2002) because the SL anomalies result from frequent large tectonic displacements of the stream bed and variable rock mass strength (Bull 2007). We use a digital elevation model (DEM) 30 m, for computing this index along every longest flow path of each basin in the Arc GIS software. The three examples of longitudinal river profile, measured SL values and their relationship with faults in the study area have shown in (Fig. 3). To show the results, we computed the average value of this index (Fig. 4a). The maximum SL value is as high as 1000 in the study area. This index varies from 7 (Subbasin 3) to 1000 (Subbasin 72). Table 1 shows the classification of the SL value index.

Drainage basin asymmetry (Af)

We applied the asymmetric factor to assess the tilting of the basins. Structural features, such as active tilting or bedding and foliation direction, play an important role and control the basin asymmetry (Pe'rez-Pen˜a et al. 2009). By using this method, we could calculate this index at the scale of a drainage basin (Hare and Gardner 1985; Keller and Pinter 2002). Definition of the asymmetric factor is as:

$$Af = 100\ (Ar/At), \text{where} \quad (2)$$

A_r is the area to the right of the main stream (looking downstream) and A_t is the whole area of the drainage basin. Af factor near of 50 shows that the basin has little or no tilting, while Af values greater or smaller than 50, indicate that the basin has affected by tectonic forces. In the study area, Af index varies from 16 (Subbasin 54) to 83 (Subbasin 6). Categorization of the Af index was into three classes: 1 ($Af \geq 65$ or $Af<35$), 2 ($35 \leq Af<43$ or $57 \leq Af<65$), and 3 ($43 \leq Af<57$) (El Hamdouni et al. 2008; Dehbozorgi et al. 2010) (Fig. 4b; Table 1).

The ratio of valley floor width to valley height (Vf)

The Vf index is one of the morphometric indices that is susceptible to tectonic uplift (Bull 2007). This index is specified as the valley floor width to valley height ratio (Vf):

$$Vf = 2V_{fw}/[(E_{ld}-E_{sc}) + (E_{rd}-E_{sc})], \text{where} \quad (3)$$

V_{fw} is the width of the valley floor, E_{ld} and E_{rd} are the altitudes of the left and right sides of the valley (facing downstream), respectively and E_{sc} is the mean altitude of the valley floor of the stream channel (Bull and McFadden 1977; Bull 1978). V-shaped valleys with low Vf values < 1 develop in response to active uplift, and that broad U-shaped valleys with high Vf values > 1 indicate major lateral erosion, due to the stability of base level or to tectonic quiescence (Silva et al. 2003). Commonly, high Vf values indicate low uplift rates (Keller and Pinter 2002). Categorization of the Vf index was into three classes: with class 1 ($Vf \leq 0.5$), for V-shaped valleys, class 3 ($Vf \geq 1$), for U-shaped valleys, and class 2 ($0.5 \leq Vf<1.0$), for intermediate cases (El Hamdouni et al. 2008). The range of Vf is from 0.35 (Subbasin39) to 3.04 (Subbasin 52) (Tables 1 and 2). The computed Vf index illustrates that almost all of the valleys in the study area are V-shaped. The location of Vf cross sections has shown in (Fig. 4c).

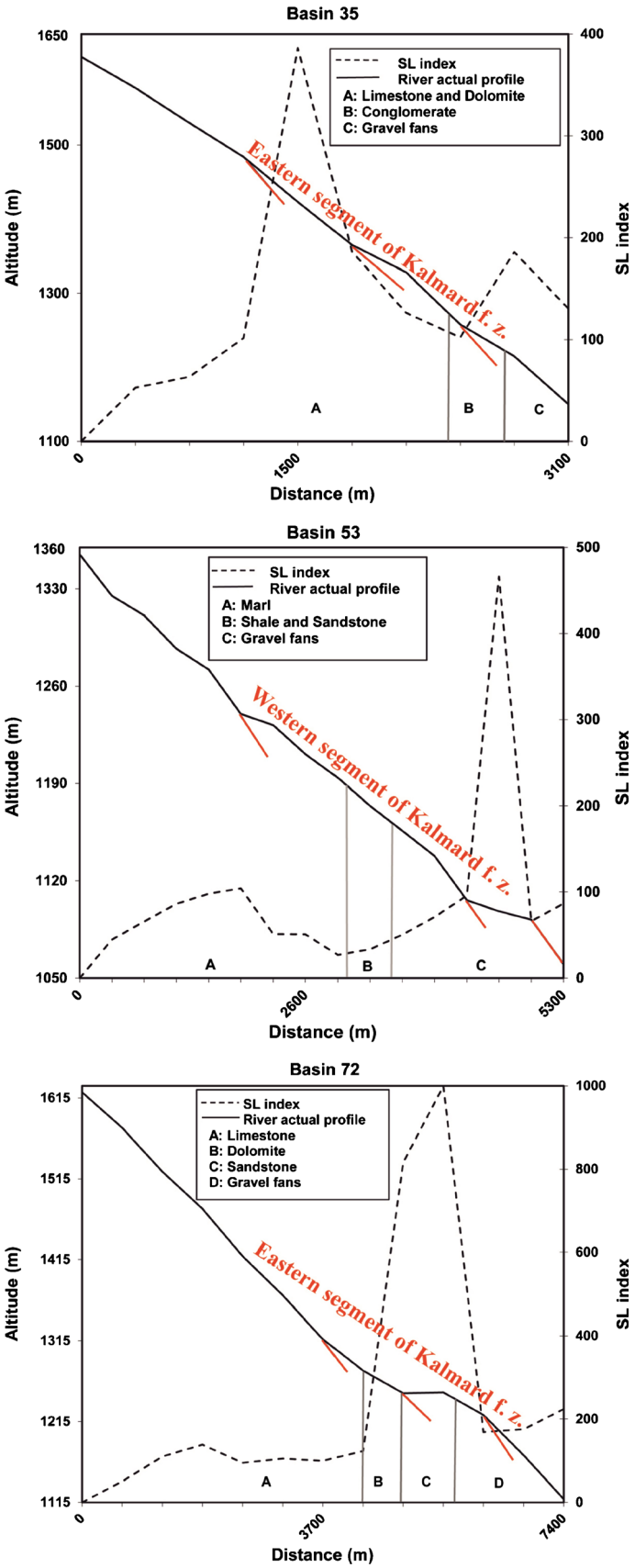

Fig. 3 Longitudinal river profiles and measured SL values for three basins in the study area

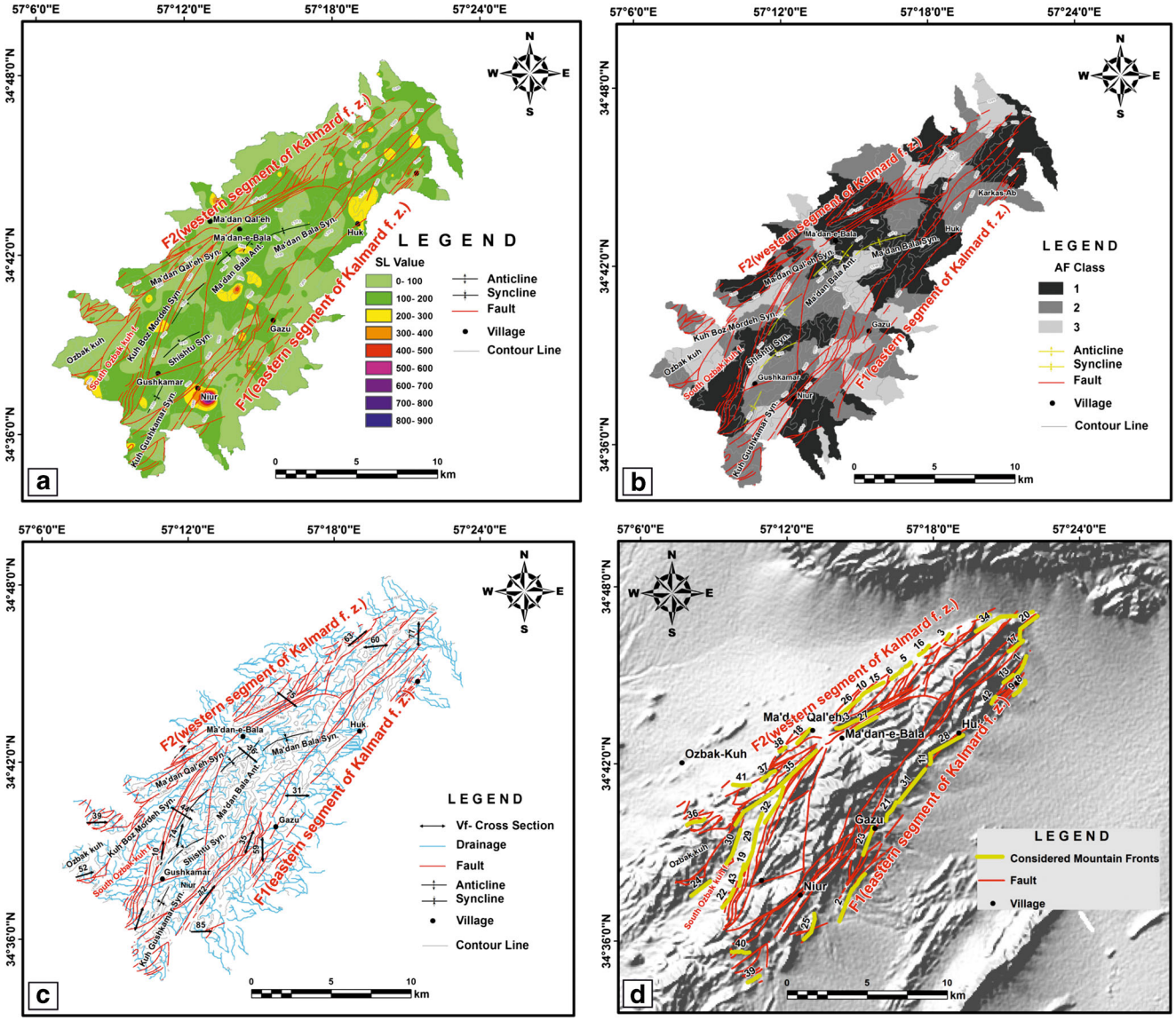

Fig. 4 The indices maps of the study area. (**a**) Stream Length- Gradient index map of study area. (**b**) Distribution map of Af classes. (**c**) Locations of sections for Vf calculations. (**d**) Thirty-five mountain-front segments for assessing the Smf index

Mountain-front sinuosity (Smf)

This index demonstrates an equilibrium between river incision processes that tend to incise the embayment into a mountain front and active tectonics forces that tend to procreate straight mountain fronts (Bull and McFadden 1977; Keller 1986; Kaewmuangmoon et al. 2008). Bull and McFadden (1977) and Bull (2007) expressed this index as:

$$\mathrm{Smf} = \mathrm{L_j}/\mathrm{L_s} \tag{4}$$

Where, L_j is the planimetric length of a mountain front along the mountain-piedmont junction, and L_s is the overall length of the mountain front. Smf is generally less than 3 and approximately 1 where steep mountains upheave swiftly along the mountain fronts (Bull 2007). Computation of the mountain-front sinuosity index was for 43 mountain fronts (Fig. 4d; Table 3) and we categorized it into three orders: 1 (Smf<1.1), 2 (1.1 ≤ Smf<1.5), and 3 (Smf ≥ 1.5) (El Hamdouni et al. 2008). The minimum value of Smf index is 1.00, and it belongs to subbasins 10, 11, and 34 (Table 3). All the values of this index belong to class 1 (Tables 1 and 3).

Hypsometric integral (Hi)

The hypsometric integral demonstrates the repartition of the altitude in an area, especially a drainage basin (Strahler 1952). Description of the Hi index is as the area beneath the

Table 1 Values of A_t (total subbasin area), the classes of SL (stream-gradient index), Af (drainage basin asymmetry), Vf (valley floor width–valley height ratio), Smf (mountain-front sinuosity), Hi (hypsometric integral) and Bs (drainage basin shape) and values and classes of Iat (relative tectonic activity)

Basin no.	Area[a] (Km^2)	SL[b] class	Af[c] class	Vf[d] class	Smf[e] class	Hi[f] class	Bs[g] class	Iat[h] value	Iat class
1	0.56	3	2	–	–	2	3	2.5	3
2	0.61	3	2	–	1	3	3	2.4	3
3	0.71	3	2	2	1	3	1	2	2
4	0.72	3	3	–	–	2	3	2.75	4
5	0.77	3	1	–	–	3	3	2.5	3
6	0.85	3	1	–	–	3	3	2.5	3
7	0.86	3	2	–	–	2	1	2	2
8	0.88	3	2	–	–	1	1	1.75	2
9	0.91	3	2	–	–	2	3	2.5	3
10	0.95	3	1	2	1	3	3	2.16	3
11	0.98	3	1	–	1	3	3	2.2	3
12	0.98	3	1	–	–	2	1	1.75	2
13	1.03	3	2	–	–	3	2	2.5	3
14	1.08	3	2	–	1	3	3	2.4	3
15	1.23	3	3	–	–	3	3	3	4
16	1.3	3	2	–	–	2	2	2.25	3
17	1.4	3	3	–	–	3	3	3	4
18	1.42	3	3	–	–	3	3	3	4
19	1.45	3	3	–	–	2	1	2.25	3
20	1.49	3	1	–	–	3	3	2.5	3
21	1.56	3	3	–	–	3	3	3	4
22	1.63	3	3	–	–	2	3	2.75	4
23	1.73	3	2	–	1	3	1	2	2
24	1.82	3	2	–	1	3	3	2.4	3
25	1.84	3	1	–	–	3	3	2.5	3
26	1.88	3	2	–	1	3	3	2.4	3
27	1.95	2	1	–	–	3	3	2.25	3
28	2.08	1	2	–	–	1	3	1.75	2
29	2.17	3	3	–	–	3	3	3	4
30	2.21	3	2	–	1	2	1	1.8	2
31	2.37	3	2	3	1	3	2	2.3	3
32	2.38	3	2	–	–	3	3	2.75	4
33	2.39	3	2	–	–	2	2	2.25	3
34	2.48	3	1	–	1	3	3	2.2	3
35	2.55	3	3	3	–	3	3	3	4
36	2.55	3	1	1	1	3	3	2	3
37	2.58	3	1	–	1	3	2	2	2
38	2.59	3	2	–	–	3	2	2.5	3
39	2.63	3	2	1	1	3	2	2	2
40	2.67	3	2	–	1	3	1	2	2
41	2.68	3	1	–	–	3	3	2.5	3
42	2.72	3	3	–	–	3	3	3	4
43	2.78	3	1	–	–	1	3	2	2
44	2.92	3	2	2	1	3	3	2.33	3
45	2.92	3	2	–	1	2	2	2	2
46	3.1	3	3	–	1	2	1	2	2
47	3.17	3	3	–	–	3	3	3	4
48	3.2	3	1	–	1	3	3	2.2	3
49	3.25	3	2	–	–	3	3	2.75	4

Table 1 (continued)

Basin no.	Area[a] (Km^2)	SL[b] class	Af[c] class	Vf[d] class	Smf[e] class	Hi[f] class	Bs[g] class	Iat[h] value	Iat class
50	3.31	3	2	–	–	3	3	2.75	4
51	3.32	3	1	–	–	1	3	2	2
52	3.33	3	2	3	1	1	3	2.17	3
53	3.6	3	1	–	1	3	3	2.2	3
54	4	3	1	–	1	3	2	2	2
55	4.07	3	2	–	1	3	2	2.2	3
56	4.13	3	1	–	–	3	3	2.5	3
57	4.3	3	3	–	1	3	2	2.4	3
58	4.4	3	1	–	1	3	3	2.2	3
59	4.43	3	2	3	1	3	2	2.33	3
60	4.59	3	2	1	1	3	2	2	2
61	4.71	3	3	–	–	3	3	3	4
62	4.88	3	2	–	–	2	1	2	2
63	5.15	3	1	1	1	3	3	2	2
64	5.34	3	3	–	1	3	3	2.6	4
65	5.44	3	1	–	1	2	3	2	2
66	5.55	3	3	–	1	3	2	2.4	3
67	6.55	3	3	–	1	1	3	2.2	3
68	0.42	3	1	–	–	2	3	2.25	3
69	7	3	1	1	1	3	3	2	2
70	7.04	3	2	–	–	3	3	2.75	4
71	7.06	3	2	–	–	3	3	2.75	4
72	7.18	1	1	2	1	3	1	1.5	1
73	7.22	3	1	–	1	3	3	2.2	3
74	7.4	3	1	2	1	3	3	2.16	3
75	8.29	3	1	2	1	3	3	2.16	3
76	8.45	3	2	–	1	3	3	2.4	3
77	8.46	3	1	1	1	3	2	1.83	2
78	9.38	3	3	–	–	3	1	2.5	3
79	1.28	3	1	–	–	3	1	2	2
80	1.43	3	2	–	–	2	1	2	2
81	0.69	3	2	–	–	2	3	2.5	3
82	1.5	3	1	–	1	3	2	2	2
83	1.12	3	2	–	–	3	1	2.25	3
84	0.42	3	2	–	–	3	1	2.25	3
85	2.35	3	1	2	1	3	1	1.83	2
86	1.29	3	1	–	–	2	1	1.75	2
87	0.9	3	3	–	–	1	1	2	2

[a] Total area of the basin

[b] Stream-gradient index

[c] Index of drainage basin shape

[d] Valley floor width-valley height ratio

[e] Index of mountain front sinuosity

[f] Hypsometric integral

[g] Index of drainage basin shape

[h] Relative tectonic activity index

Table 2 Vf table associated with lithology of the valley floor

River no.	Basin area (Km^2)	Lithology of the valley floor	Vf index[a]	Vf class
3	0.71	Conglomerate and Sandstone	0.81	2
10	0.95	Shale, Sandstone and Limestone	0.65	2
31	2.37	Limestone, Sandstone and Shale	1.32	3
35	2.55	Limestone and Sandstone	1.02	3
36	2.55	Limestone and Dolomite	0.50	1
39	2.63	Shale and Sandstone, Limestone	0.35	1
44	2.92	Shale and Sandstone	0.56	2
52	3.33	Limestone	3.04	3
59	4.43	Dolomite	2.63	3
60	4.59	Limestone	0.42	1
63	5.15	Dolomite	0.47	1
69	7.00	Limestone and Dolomite	0.46	1
72	7.18	Limestone, Sandstone	0.72	2
74	7.40	Shale and Sandstone	0.85	2
75	8.29	Marl, Shale and Sandstone	0.93	2
77	8.46	Limestone and Shale, Sandstone	0.49	1
85	2.35	Shale and Sandstone	0.98	2

[a] Valley floor width-valley height ratio

hypsometric curve. The equation used for computing the Hi index (Pike and Wilson 1971; Mayer 1990) is:

$$Hi = (Average\ elevation–min\ elevation/max\ elevation–min\ elevation). \quad (5)$$

In this index, we acquired the maximum, minimum, and average altitudes from digital elevation model (DEM) using the Arc GIS software. After computing the Hi index for all of the drainage basins, this index was ordered into three classes: class 1 with convex curves ($Hi \geq 0.5$); class 2 ($0.4 \leq Hi < 0.5$); and class 3 with concave curves ($Hi < 0.4$).The greatest value of hypsometric integral corresponds to subbasin 67 (0.58) (class 1).In the study area the Hi index ranges from 0.21 (class 3) (Subbasin 78) to 0.58 (class 1) (Subbasin 67) (Table 1).

Basin shape index (Bs)

Basins shape can change due to tectonic activity. The basin shape index illustrates discrepancy between basins with considerable elongation and basins with nearly roundish shape. The basin shape index or the elongation ratio (Ramirez-Herrera 1998) may describe the horizontal projection of a basin. The Bs index is determined as (Cannon 1976; Ramirez-Herrera 1998):

$$Bs = Bl/Bw \quad (6)$$

Where, Bl is the length of a basin computed from the most elevated point, and Bw is the width of the basin measured at its widest point. Calculation of the Bs index was for all drainage basins and we ordered it into three levels: 1 ($Bs \geq 4$), 2 ($3 \leq Bs < 4$), and 3 ($Bs \leq 3$) (El Hamdouni et al. 2008). Computation of the Bs index was for all subbasins. Table 1 shows the results of this index. Bs index ranges from 0.9 (Subbasin 67) to 5.01 (Subbasin 12). About 60% of the studied subbasins belong to class 3 with nearly circular shapes (Table 1).

Calculation of Iat

Previous studies on relative tectonic activity based on geomorphic indices tend to focus on a particular mountain front or area (Bull and McFadden 1977; Rockwell et al. 1985; Azor et al. 2002; Molin et al. 2004). In this article, we utilize a number of morphometric indices to assess tectonics in the study area. To obtain more precise results, the six indices divided into four classes, and each class assigned a weighting value. These classes summed and averaged to obtain an Iat over the entire study area. Iat is defined as:

$$Iat = (SL + Af + V_f + Smf + Hi + Bs)/6 \quad (7)$$

For describing the degree of active tectonics, we distributed this index into four categories: 1–very high ($1.0 \leq Iat < 1.5$); 2–high ($1.5 \leq Iat < 2.0$); 3–moderate ($2.0 \leq Iat < 2.5$); 4–low ($2.5 \leq Iat$) (El Hamdouni et al. 2008). The distribution of the four classes is shown in Fig. 5, and Table 1 shows the result of the classification for each subbasin.

Table 3 Values and classes of Smf (mountain-front sinuosity) for the considered mountain fronts

Mountain front no.	Basin no.	Smf[a]	Class
1	76	1.01	1
2	66, 79, 80, 81	1.05	1
3	63	1.04	1
4	34	1.00	1
5	76	1.01	1
6	76	1.01	1
7	73	1.06	1
8	73	1.03	1
9	23	1.02	1
10	75	1.02	1
11	54	1.02	1
12	60, 64	1.01	1
13	23, 73	1.01	1
14	73	1.04	1
15	75	1.06	1
16	63	1.03	1
17	73, 77	1.01	1
18	30, 37	1.01	1
19	10, 11, 34	1.00	1
20	77	1.01	1
21	24, 46	1.02	1
22	69	1.01	1
23	35, 45, 59	1.01	1
24	52, 67, 69	1.01	1
25	72	1.04	1
26	53, 75	1.02	1
27	65	1.02	1
28	54	1.02	1
29	10, 44, 74	1.01	1
30	2, 14, 57, 67	1.01	1
31	31, 48	1.01	1
32	44, 57	1.01	1
33	53, 65, 75	1.03	1
34	60, 64, 77	1.01	1
35	26, 57	1.02	1
36	39	1.02	1
37	58	1.01	1
38	3	1.01	1
39	55	1.02	1
40	55	1.02	1
41	58	1.01	1
42	40	1.01	1
43	34	1.00	1

[a] Index of mountain front sinuosity

Appraisal of relative tectonic activity

The average of the six measured geomorphic indices (Iat) was used to evaluate the distribution of relative tectonic activity in the study area (El Hamdouni et al. 2008). The Iat index classes computed within the study area as follows: about 3% (7 Km^2) is class 1 (very high relative tectonic activity); 27% (71 Km^2) is class 2 (high relative tectonic activity); 50% (131 Km^2) shows moderate values of tectonic activity (class 3), and 20% (52 Km^2) has the lowest values of relative tectonic activity (class 4) in the study area (Fig. 5; Table 1). Almost all the values of Iat tend to be mostly high and partially moderate along the east Kalmard fault zone segment (F1) (Fig. 6a) and Iat values in the western segment of Kalmard fault zone (F2) (Fig. 6b) tend to be mostly moderate and partially high, but the central strip of the Ozbak-Kuh mountains has low values of tectonic activity (Fig. 5).

Normalized steepness index (Ksn) and Knickpoints

The analysis of the longitudinal profile of rivers can provide useful information in association with climate changes and tectonic (Hack 1957; Whipple et al. 2013). The river profile is presented based on the relationship between the channel slope (S) and the upstream area of the basin (A) which is introduced as the law (Flint's Law) (Flint 1974):

$$S = k_s A^{-\theta} \tag{8}$$

In this equation (s) is the amount of steepness, (ks) is the steepness index, (A) is area, and (θ) is the concavity index. Different values of the steepness index (ks) along the river indicate a change in the river's creep rate due to the variability of the erosion of the channel floor sediments and the uplift of the bedrock (Kirby et al. 2003). The value of the steepness index (KS) and the rate of erosion or uplifting of the bedrock in a steady state is obtained from the following equation:

$$K_S = (E/K)^{1/n} \tag{9}$$

In the above eq. (E) is bedrock uplift, (K) indicates the erosion coefficient that depends on the climatic and metamorphic conditions of the area and (n) is a positive exponent related to the dominant erosion process in the area. (Kirby et al. 2003; Wobus et al. 2006). Different rates of uplifting of the area in the regions with a stable river profile where river vertical digging balances the uplift is well illustrated by this equation (Kirby and Ouimet, 2011). There is a strong correlation between the amount of concavity (θ) and the steepness index (ks). Any change in the amount of the concavity index causes a wide variation in the value of the steepness index. To adjust the amount of concavity and compare the different longitudinal profiles the steepness index is normalized according to the

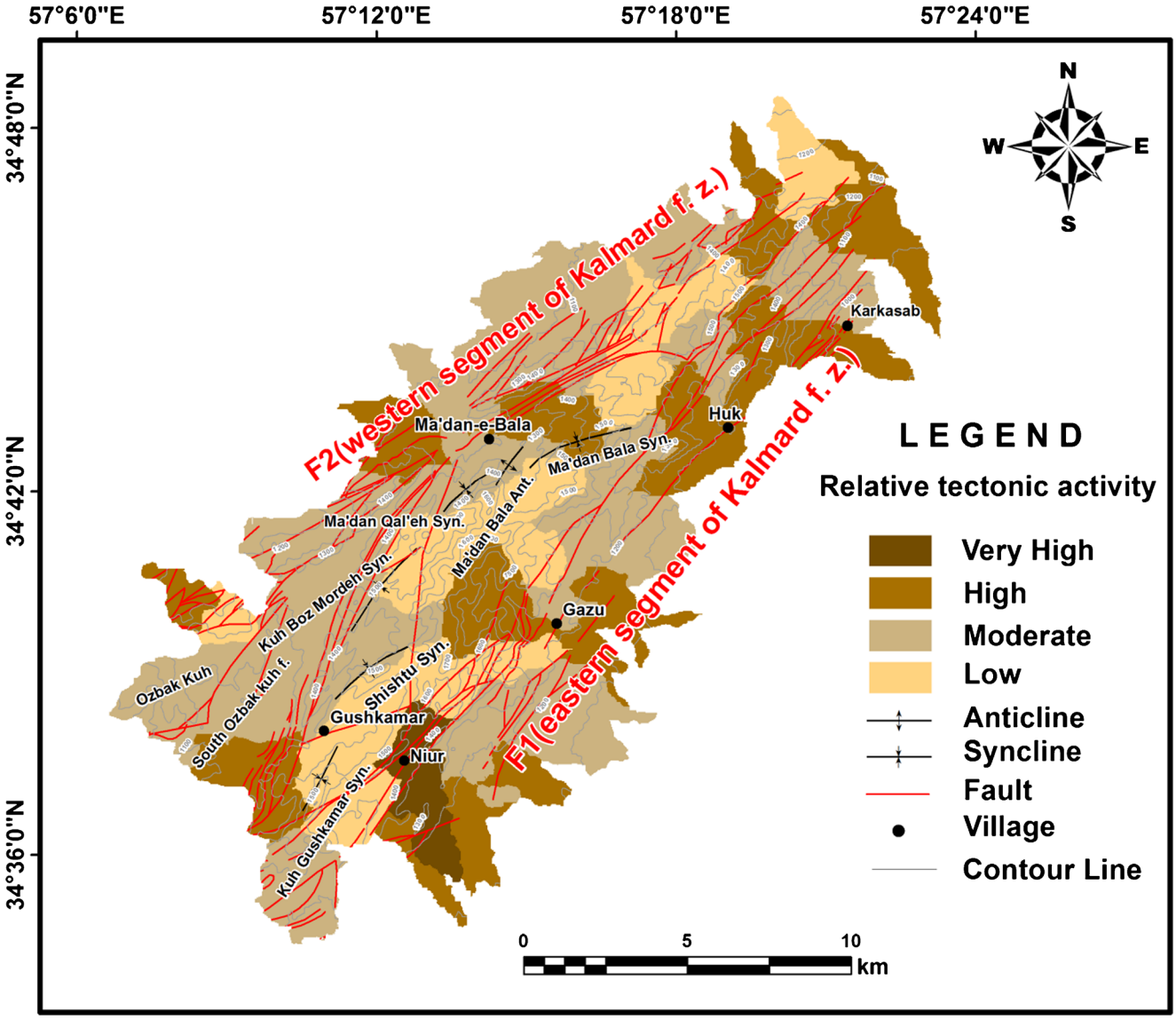

Fig. 5 Distribution of Iat classes

reference concavity index (θ_{ref}((Kirby and Whipple, 2001). In order to further validate the results the normalized steepness index (Ksn) is calculated with the reference concavity index value which is 0.45. In this study the steepness and concavity with the amount of reference concavity index are obtained in Matlab software. The results of the relative steepness index in the studied basins are shown in Figs. 7, 8, and 9 that concave index also indicates the uplift of the rivers in these basins.

A part of the longitudinal profile of the river which is more precipitous than adjacent parts is known as the knickpoint often seen along bedrock rivers and is more visible in the streams with flow in the form of water fall (Hayakawa and Oguchi, 2009; Hayakawa and Matsukura, 2003). The knickpoint are often formed abundantly in the precipitous section and near the sources of the rivers, and it is thought that the hydrological conditions affect their creation. Another factor contributing to the formation of knickpoints is active tectonic (Hayakawa and Oguchi, 2009). The effect of active tectonics on the rivers is surveyed in this study. The position of the faults on the longitudinal profiles, without considering their dip and strike, was done to investigate the relationships between the faults in creating the knickpoints (Fig. 10). In this study, likewise, the effects of the major and important faults (F1 to F6) on multiple longitudinal profiles were investigated (Figs. 7, 8 and 9).

Field work data

In the Ozbak-Kuh area, a number of major faults including F1 to F6 (Fig. 1c) are considered as the Kalmard fault zone strand. Based on field studies, the rose diagram of the strand

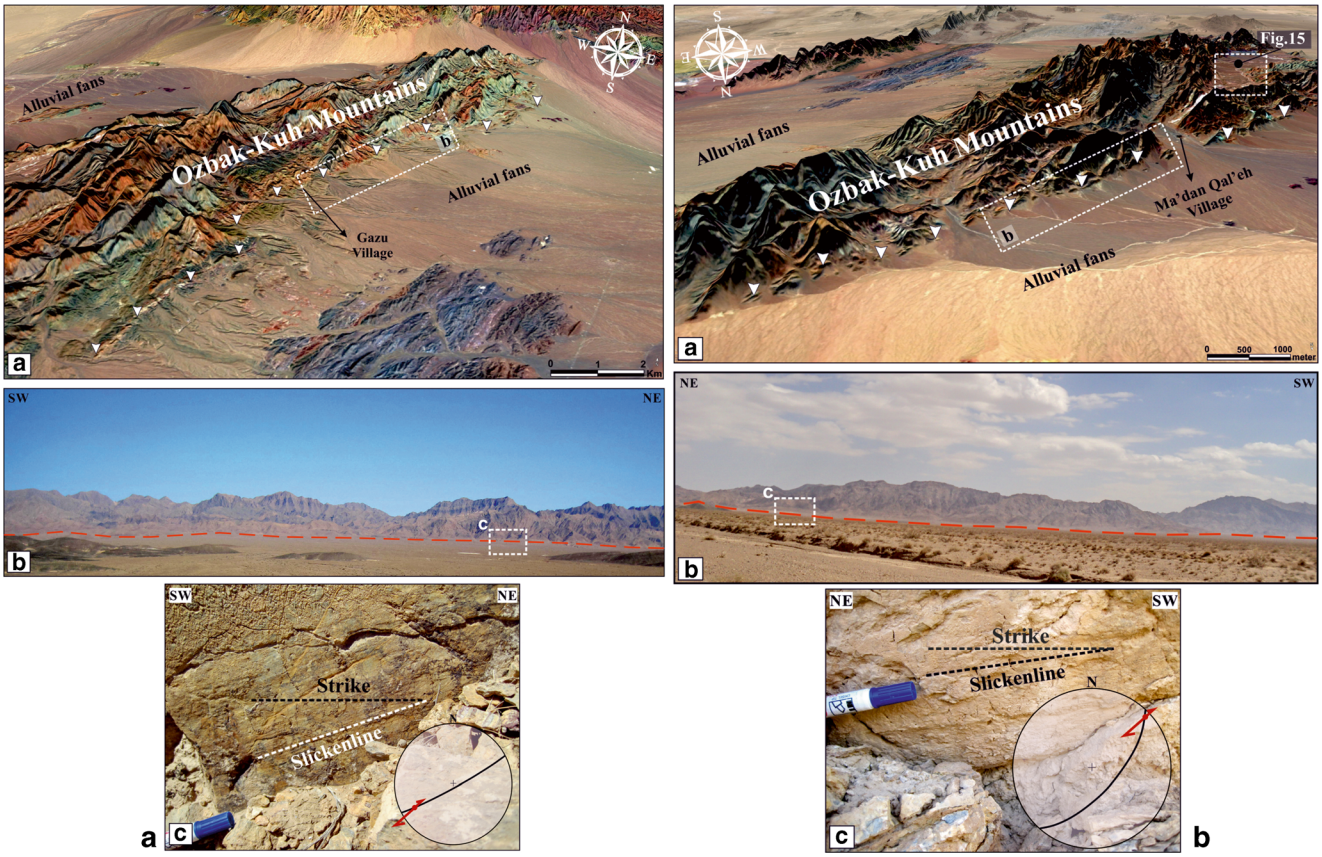

Fig. 6 **A** The mountain front in the eastern segment of Kalmard fault zone (fault F1), Ozbak-Kuh area. (**a**) Prospective view from satellite image (source: http://earth.google.com). (**b**) Field photo of the straight mountain front along the fault F1. (**c**) Detail of the polished fault F1 surface of the fault shown in (**b**) with subhorizontal slickenlines with stereoplot (Schmidt net, lower hemisphere projection) showing the right lateral fault F1 data. **B** The mountain front in the western segment of Kalmard fault zone (fault F2), Ozbak- Kuh area. (**a**) Prospective view from satellite image (source: http://earth.google.com). (**b**) Field photo of the straight mountain front along the fault F2. (**c**) Polished subvertical fault F2 surface with subhorizontal slickenlines with stereoplot (Schmidt net, lower hemisphere projection) showing the right lateral fault F2 data

of Kalmard fault zone (F1 to F6) was made in which the average trend is N38E (Fig. 1c). These faults present some geomorphic evidences which can show their potential activity in the future.

Fault F1

This fault is known as the eastern segment of the Kalmard fault zone in the Ozbak-Kuh area is located in the east of the studying area (Fig. 1c). Considering that fault F1 separates Quaternary sediments from Paleozoic rocks, it is considered as a mountain front fault in the eastern parts of the Ozbak- Kuh Mountains. Fault F1 coincide with a straight mountain front that has been classified as class 1 in the classification of mountain-front sinuosity index. The collected data indicates a strike of 062° and a dip of 85° to the SE with a rake angle of 20° (from southwest) (160° clockwise with respect to the right hand rule strike and positive dip). Regarding the slicken-lines on the fault plain, the movement of this fault is identified as right lateral strike-slip with a normal component (Fig. 6a).

Fault F2

Fault F2 represents the western segment of the Kalmard fault zone and is situated in the western part of the Ozbak-Kuh Mountains (Fig. 1c). Similarly to the fault F1, it separates Quaternary from Paleozoic units and coincides with a linear front. The fault F2 has an orientation of 042/70 SE and a rake of 12° (from northeast). Based on the slicken-lines on the fault plain, the movement of this fault is right lateral strike-slip with a reverse component (Fig. 6b).

Fault F3

Fault F3 with a length of 5 km (Fig. 1c) and a dip of 80° to the northwest has an average strike of 040°. Movements of this fault have placed limestones and shales of the Niur Formation (Silurian) in contact with sandstones and dolostones of the Padeha Formation (Devonian). The observed S-C structures in the vicinity of this fault and the

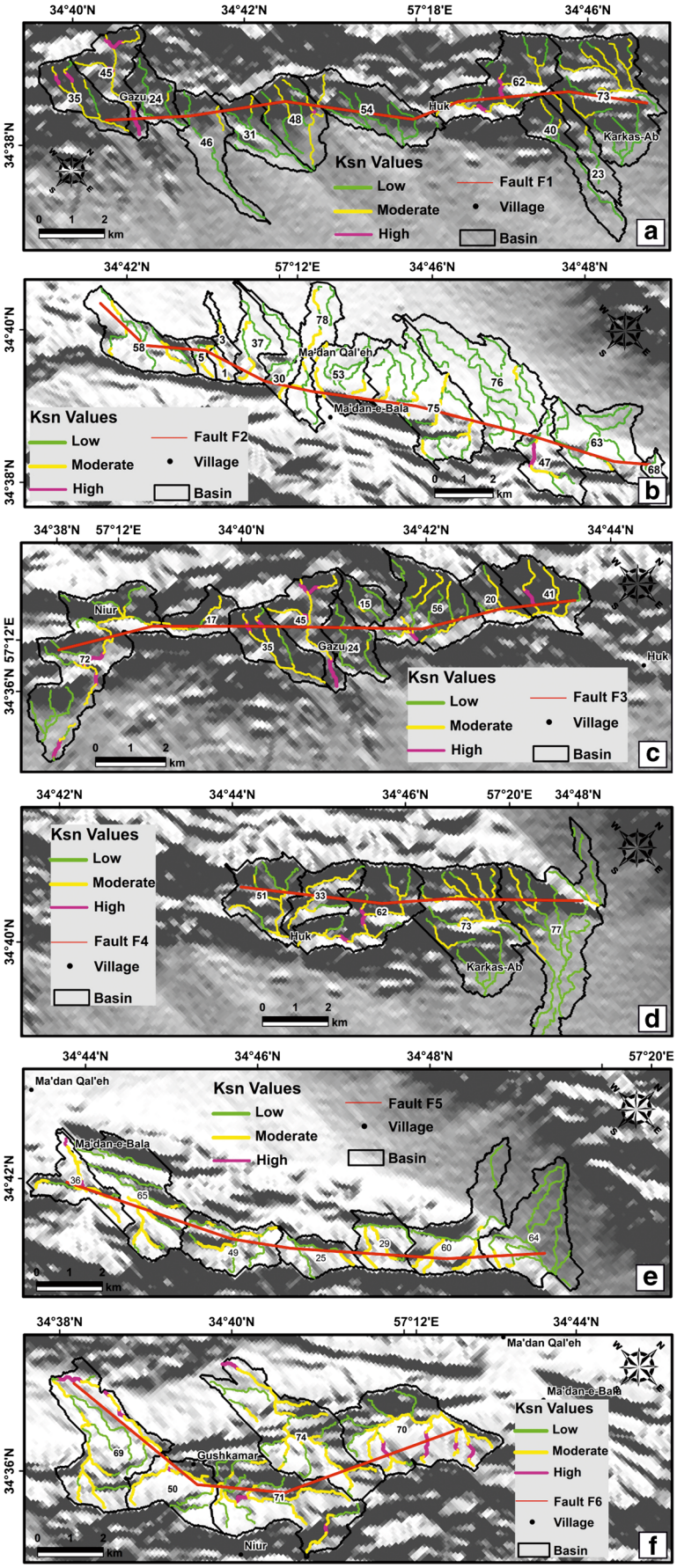

Fig. 7 Normalized steepness index (Ksn) maps on the faults of the study area. (**a**) Ksn map on the fault F1, (**b**) Ksn map on the fault F2, (**c**) Ksn map on the fault F3, (**d**) Ksn map on the fault F4, (**e**) Ksn map on the fault F5, (**f**) Ksn map on the fault F6

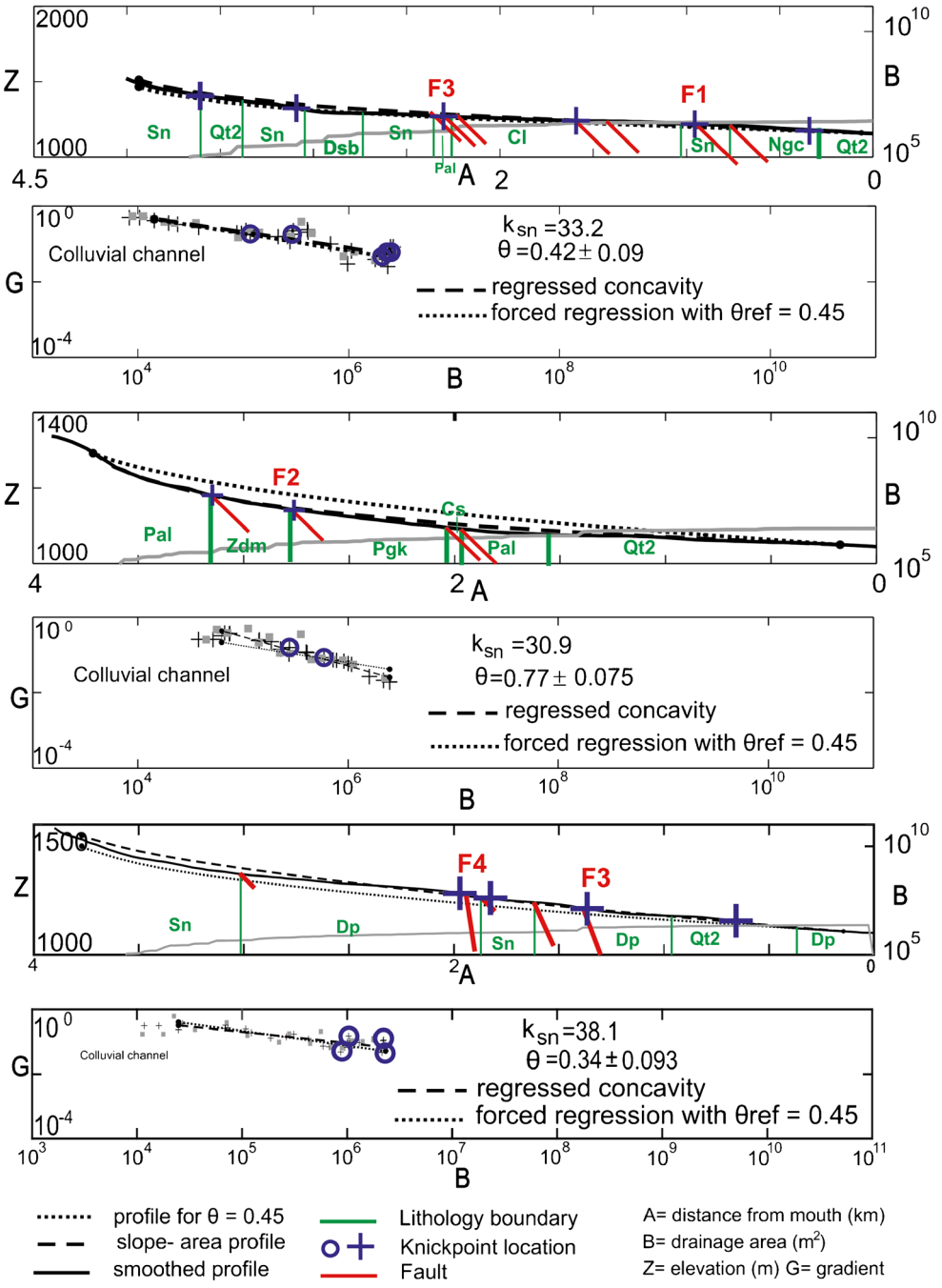

Fig. 8 Longitudinal river profiles on the faults F1-F3

slicken-lines with a rake of 10–15° associated with riedel fractures point to a right lateral strike-slip mechanism with a reverse component. The collected data on fault plains and the locations of the slicken-lines are shown in a Streograph (Fig. 11).

Fault F4

Fault F4 with an approximate length of 12 km (Fig. 1c) has an average dip of 77° toward the southeast and an average strike of 050°. With regard to the data collected in numerous parts of the fault plain during the field observation such as fault steps, riedel fractures, slicken-lines, and S-C structures, this fault presents a right lateral strike-slip fault kinematics with a reverse component (Fig. 12).

Fault F5

Fault F5 with a relative length of 8 km (Fig. 1c) separates gray limestones of the Bahram formation (Devonian) from

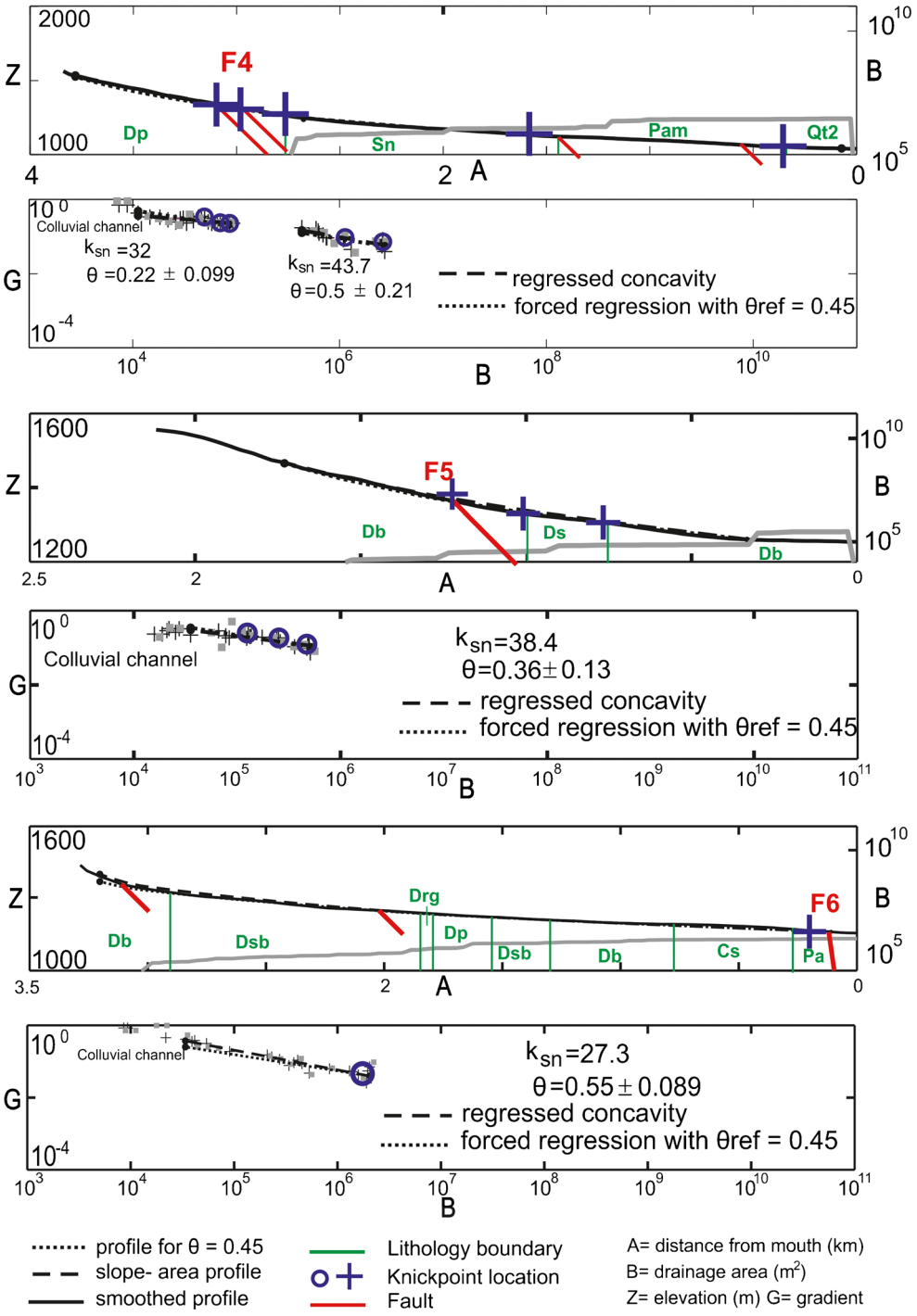

Fig. 9 Longitudinal river profiles on the faults F4-F6

the red sandstones of Lalun formation (Cambrian). The aforementioned fault has an average strike of 035° and dips 82° toward the northwest. The observed slicken-lines on the fault plain have an average rake of 20 degrees which are associated with extensional fractures. Moreover, the S-C structures observed in the vicinity of this fault, demonstrate a right lateral strike-slip kinematics with a reverse component. The mentioned reverse component has caused the juxtaposition of Cambrian sandstones over Devonian limestones (Fig. 13).

Fault F6

This fault has a length of 5 km (Fig. 1c). Fault F6, separates the Sardar formation (Carbonifer's shale and sandstones) from the Padeha formation (Devonian's sandstones). The

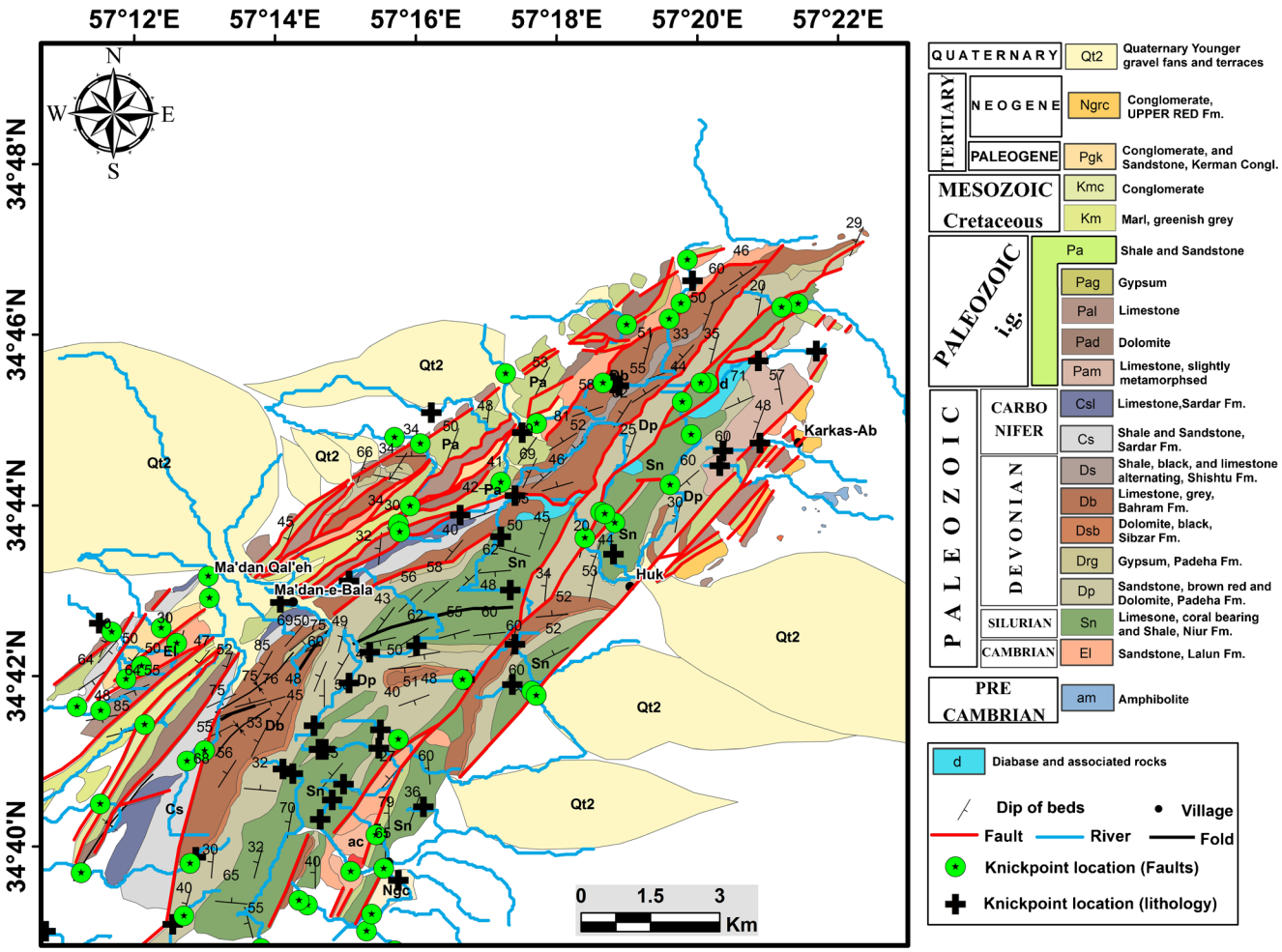

Fig. 10 Knickpoints location on the geological map in the Ozbak-Kuh area

movement of this fault is right lateral strike-slip with a reverse component.

Evidence of quaternary deformation

Deformation related to above faults is documented by the general presence of Quaternary fracturing (Fig. 14a–d), deformed Quaternary deposits (Fig. 15), straight mountain front (Figs. 4d and 6; Tables 1 and 3) and our Iat analysis (classes 1, 2) (Fig. 5; Table 1). The presence of faults and fractures in the Quaternary deposits seem to be very important, because they can indicate the active tectonics of this region. Fractured river terraces and consolidated alluvium were surveyed through field studies. Consequently, we measured the direction of the 109 Quaternary fractures occurring in the different parts of the study area on the Kalmard fault zone (Fig. 14). According to field investigations, the average trend of the Kalmard fault strand (F1 to F6) is as N38E (Fig. 1c). Based on structural studies and field evidences, we constructed the Rose Diagram of Quaternary fractures cutting the apex zone of some terraces (Fig. 14e). Accordingly, the direction of their averages is N26E, which is parallel to the common direction of Kalmard Fault zone. Quaternary deformation evidences are well exposed in some parts of the area as the elevation of the consolidated alluvial terraces reaches to 15 m due to a deep cut through the channel course. We can see an illustrative example around the Gushkamar village (Fig. 14a) where some high-steep fractures cut both the Quaternary alluvium and the underlying Lower Cretaceous deposits. Likewise, Around the Maadan Qaleh village (Fig. 14b), Paleozoic rocks have been down cut by the river and have made a strath; so that these rock units are cropped out through the walls and floor of the river, and the Quaternary alluvial terraces lied on them. The faults and fractures of the Kalmard fault zone have ruptured both the Paleozoic and the overlying Quaternary rock units. Furthermore, in some parts of Ozbak-Kuh, it can be seen that the Quaternary alluvial terraces have an average strike of 020° and dips 32° toward the northwest, are tilted 32° northwestward (Fig. 15). This represents the effect of F6 fault in Quaternary unit's deformation in this part of study area. Furthermore, some morphotectonic landforms such as straight mountain fronts (Figs. 4d and 6), well-developed triangular

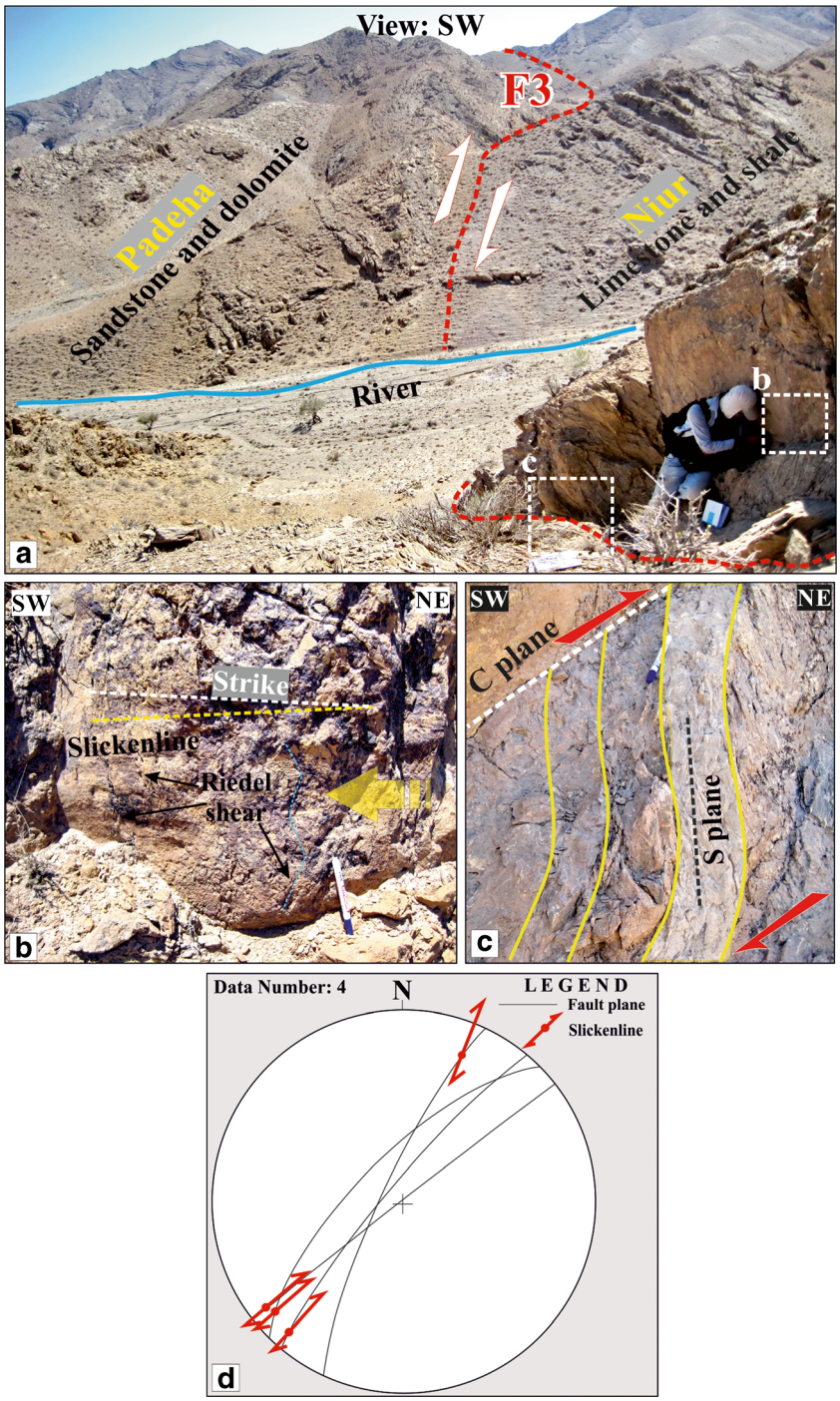

Fig. 11 Characteristics of fault F3. (**a**) Field photo of the fault F3. (**b**) fault sarface slickenlines and synthetic riedel shear fractures indicating the right-lateral kinematics along the fault F3 plane. (**c**) S-C structures related to fault F3. (**d**) Stereoplot showing the collected fault F3 data, striae as arrows

facets (Fig. 16a), deep and narrow gorges (Fig. 16b) incised into mountain fronts along the fault strand and knickpoints (Fig. 16c) were measured and investigated in the field studies.

Discussion

The present study focuses on Ozbak-Kuh area (Kalmard Fault Zone, Central–East Iran) where no earthquakes have been recorded. However, there exist several evidences related to recent tectonic activity like knickpoints, ruptured terraced alluvium and active landforms. Without doubt, the creation of tectonic landforms in the Ozbak-Kuh area is largely rooted in the recent movements along Kalmard fault zone strand in this part of Iran. The Kalmard fault zone is a 250-km long zone that consists of NE–SW striking fault segments, runing on Kashmar–Kerman tectonic zone in the Central Iranian plate. The present-day stress state obtained from earthquake focal

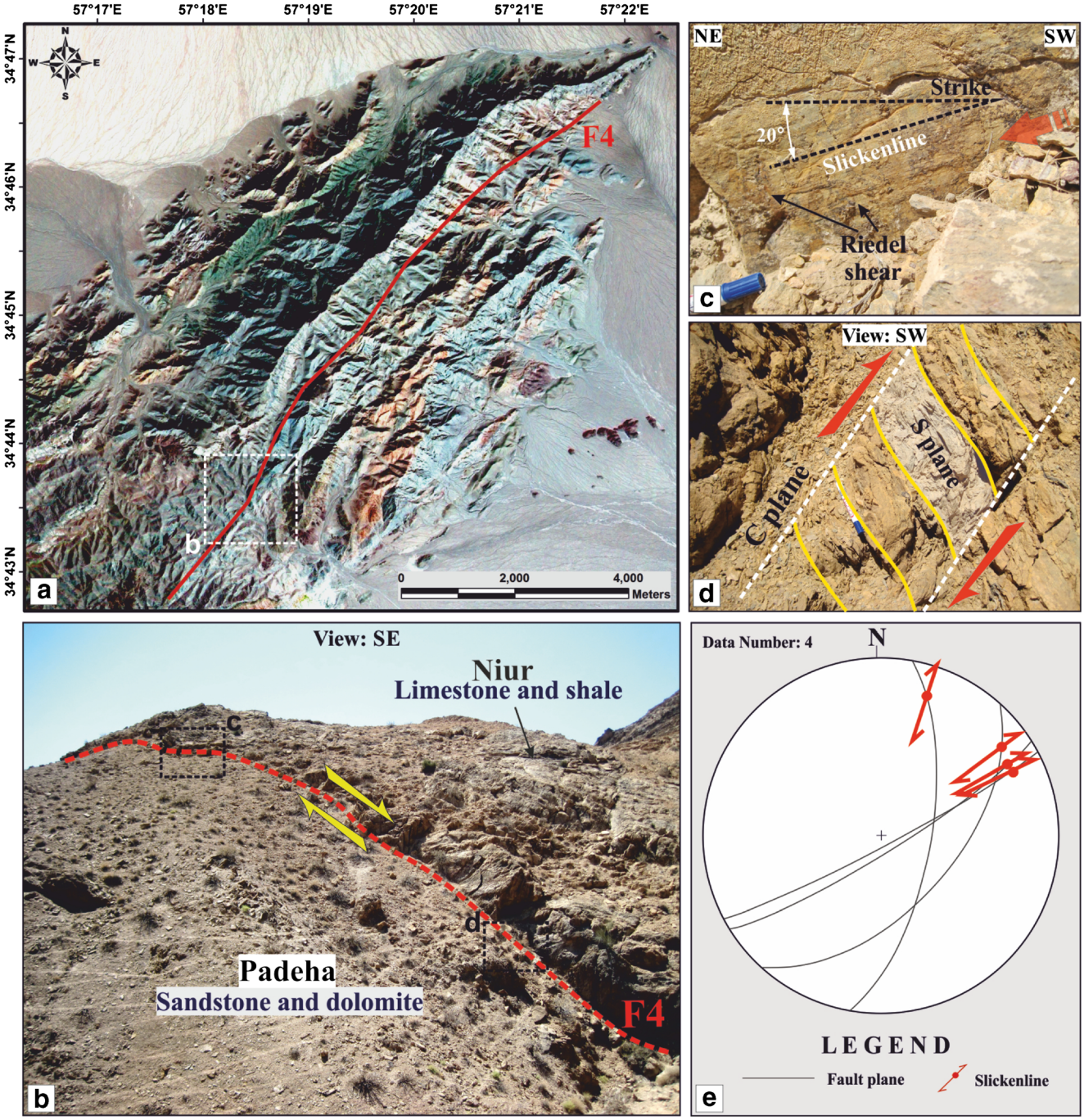

Fig. 12 Characteristics of fault F4. (**a**) IRS P5 Satellite image. (**b**) Field photo of the fault F4. (**c**) Slickenlines and riedel shear fractures on the fault F4 plane. (**d**) S-C planes representing the right-lateral kinematics along the fault F4. (**e**) Stereoplot (Schmidt net, lower hemisphere projection) showing the fault F4 planes, striae is marked by arrows

mechanisms shows that the North of Central–East Iran Blocks (NCEIB) is presently subjected to a transpressional tectonic regime ($R' = 1.78 \pm 0.26$), with a N37 ± 7°E direction of horizontal principal compression (Naimi-Ghassabian et al. 2015). The resulting stress tensor suggests that compression is homogeneous in a NE–SW orientation (N38 ± 8.8°E), and the expression of the combination of thrust and strike–slip faulting has caused by the relatively high stress ratio R' (2.00 ± 0.31) (Naimi-Ghassabian et al. 2015). This stress state is consistent with the direction of convergence between the Arabian and Eurasian plates and leads to the recent active tectonics of the study area. The structural and geomorphic investigation revealed the evidence of prominent Quaternary transpression kinematics along the NE–SW segments of Kalmard fault zone. Faulting mainly localizes along the range fronts, likely reactivating preexisting structures in the bedrock, and

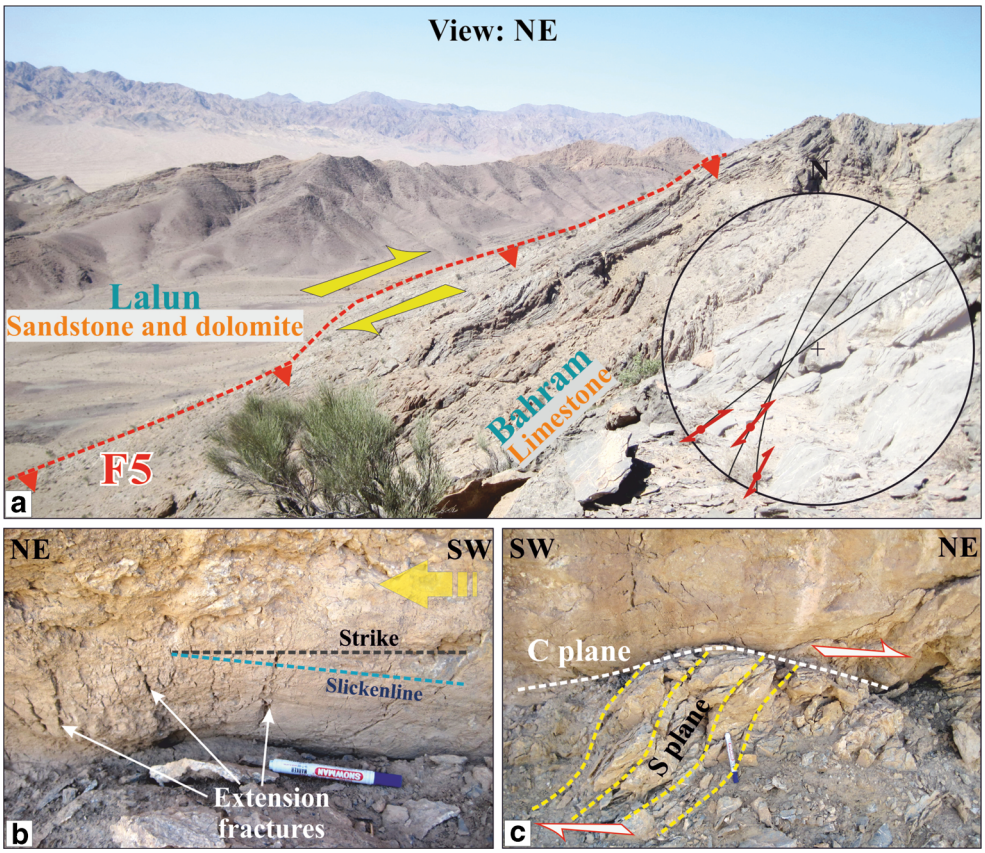

Fig. 13 Attributes of fault F5. (**a**) Field photo and stereoplot showing the fault F5 data, striae as arrows. (**b**) slickenlines and extension fractures indicating the right-lateral kinematics along the fault F5. (**c**) S-C structures associated with fault F5

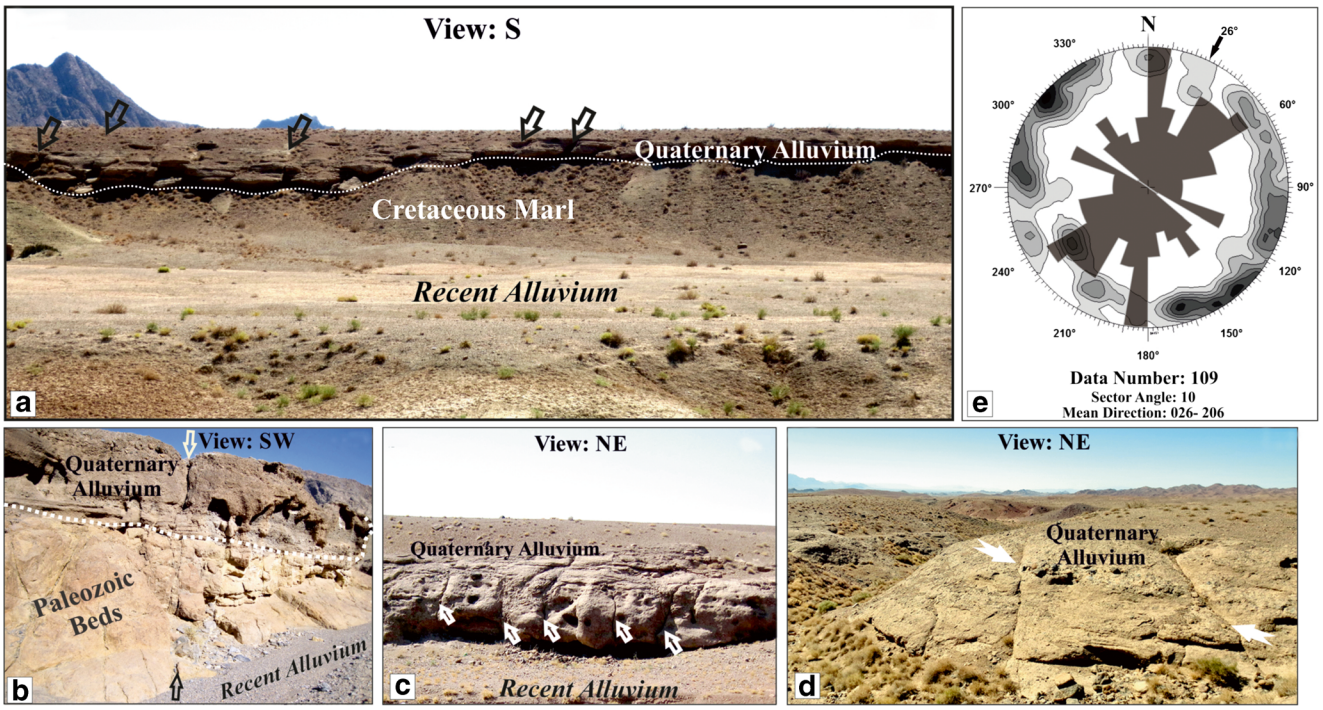

Fig. 14 Quaternary faulting and fracturing along the Kalmard fault zone in different parts of Ozbak-Kuh area. Fractures is marked by arrows. (**a**) Faults and fractures affecting the Quaternary deposits at Gushkamar village. (**b**) Truncated Paleozoic rock units and fractured Quaternary alluvial deposits (terraces) due to the Kalmard fault zone activity near Ma'dan Qal'eh village. (**c**) Fracturing of consolidated Quaternary deposits through steeply incised drainages in Gazu village. (**d**) Quaternary faulting and fracturing in the Kalmard fault zone at Niur village. (**e**) Rose diagram and Contour diagram of the cumulative fracture strike data in the Quaternary deposits of the Kalmard fault zone

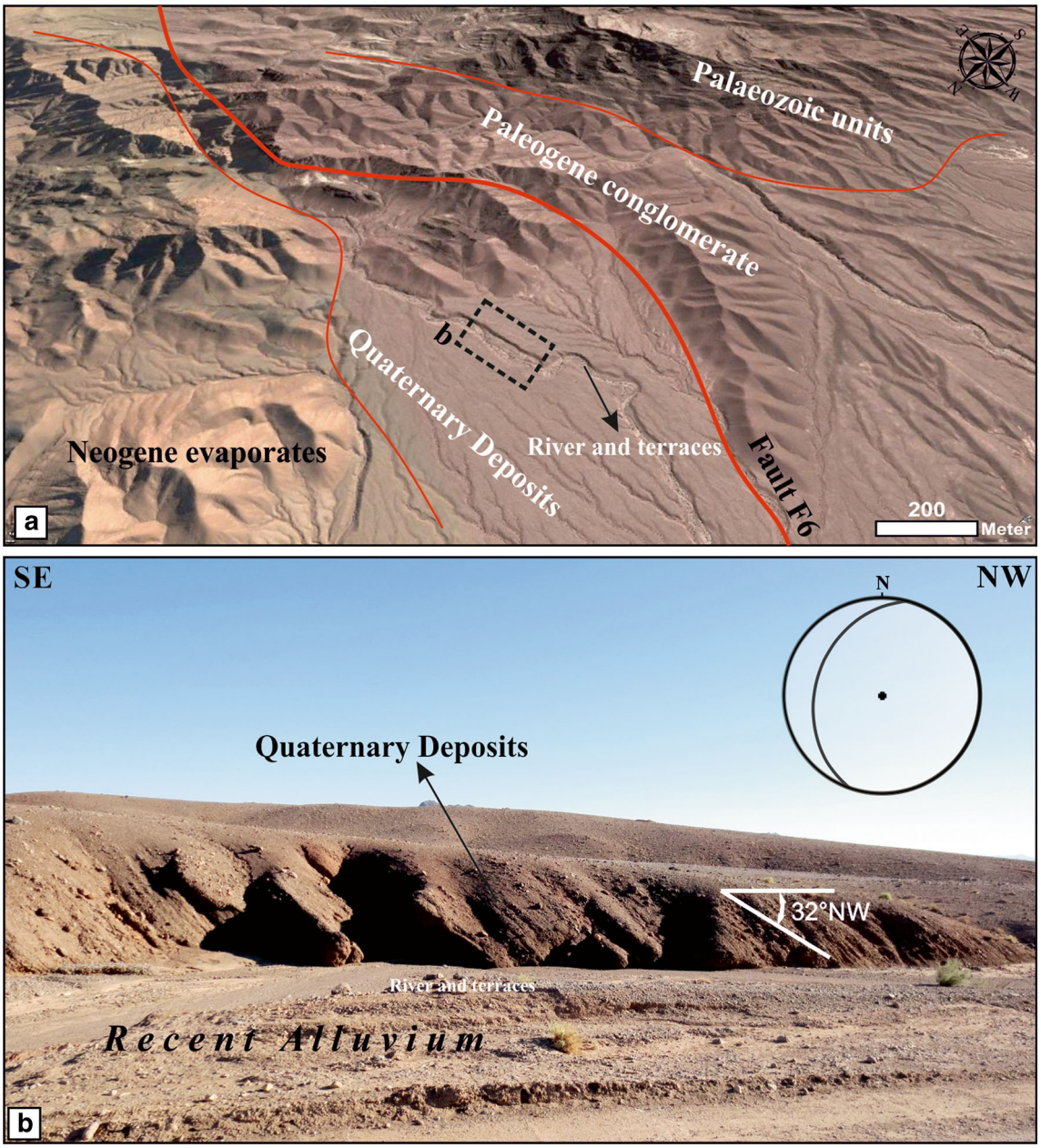

Fig. 15 Young deformed Mio-Pliocene-Quaternary alluvial deposits. (**a**) Prospective view from satellite image (source: http://earth.google.com) is showing the relationship between fault F6, river, terraces and recent alluvium deposits. (**b**) Field photo of deformed recent alluvium near Niur village in the southern part of the study area

suggesting a strong control operated by older geological structures on the post-Neogene fault pattern in Central Iran (Walker and Khatib 2006). Although there are no absolute ages of alluvial fans, we can regionally compare them to similar deposits from Central Iran. Thus, we used the regional scenario and some more detailed data on age of the deformation in neighbor areas based on optically stimulated luminescence dating of three generations of alluvial fans and fluvial terraces. We have used it as a reference for provisional age correlations which reconstructed by Calzolari et al. (2016) for the Central eastern Iran. These ages are related to the recent alluvial deposits that have cut by faults. Three age clusters for aggradation phases can be recognized at ~6, ~25, and ~53 ka, respectively, which correspond the regional ages obtained for Central Iran (Walker and Fattahi, 2011). Deposition of the Shesh–Taraz river terrace along the Doruneh Fault (situated in the northeastern part of the study area) has the age of 20.1 ± 1.5 ka (end of the Last Glacial Maximum) and Fattahi et al. (2007) obtained it using an IRSL (infrared-stimulated luminescence) method. Forthermore, the age of the younger faulted deposits (~5 ka) constrains the minimum age of right lateral faulting in the Kuh-e-Sarhangi (KSF) and Kuh-e-

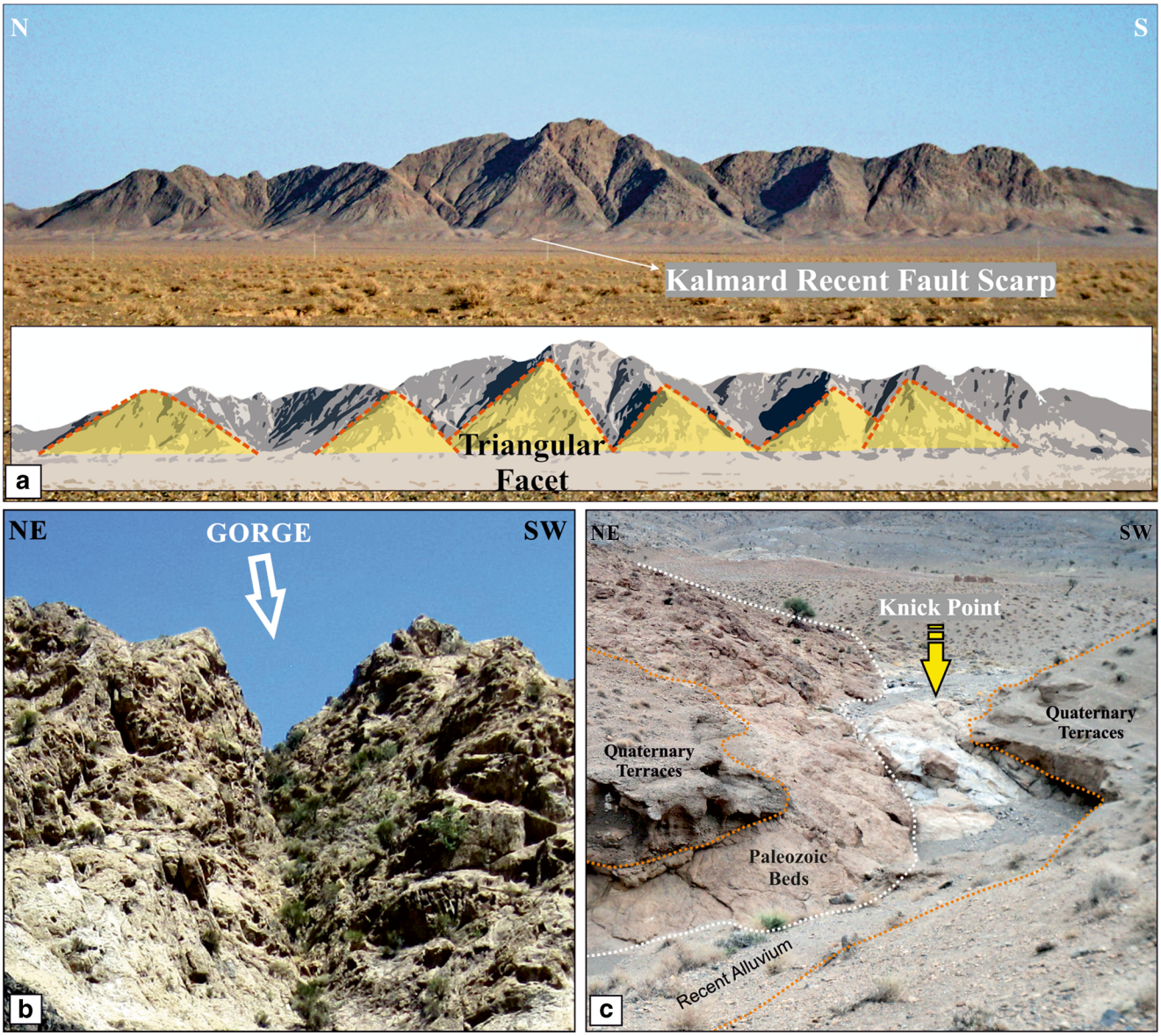

Fig. 16 Morphotectonics landforms in the study area. (**a**) Triangular facets along the fault F1 (the eastern segment of Kalmard fault zone). (**b**) A deep gorge cutting the limestone units in Gazu village. (**c**) A knickpoint on the longitudinal profile of a stream due to fault movements near Ma'dan Qal'eh village

Faghan Fault (KFF) systems (situated in the north of Ozbak-Kuh) to the Holocene at the northern edge of Lut Block (Calzolari et al. 2015). The OSL and structural data set on the Quaternary deposits along the KSF-KFF fault zone shows that strike-slip tectonics and related localized uplift occurred post ~50 ka through Holocene, with a general progression of fault zone localization and slip along eastward propagating KFF (Calzolari et al. 2016). Three generations of Quaternary alluvial fans and river fill terraces associated with the dismantling of the fault-related topographic relief were recognized and dated by means of OSL at ~53, ~25, and ~6 ka, respectively (Calzolari et al. 2015). Forthermore, right lateral strike-slip tectonics was represented for the Kuh-e-Faghan Fault (KFF) (east of the Kuh-e-Sarhangi Fault) by Calzolari et al. (2015). The study has done for the first faulting/exhumation episode based on the structural and depositional architecture of the Neogene deposits in the Kuh-e-Faghan Fault (Calzolari et al. 2016). They are correlated with the regionally defined Late Quaternary aggradation and abandonment phases previously recognized over Central Eastern Iran in other studies. Such dates constrain to the Holocene the minimum age of faulting along the KSF-KFF right lateral strike-slip system at the northern edge of Lut Block (Calzolari et al. 2015). Also, post Neogene right lateral strike-slip faulting has documented at the north-western edge of the Lut Block in the Kashmar-Kerman Tectonic Zone by Nozaem et al. (2013). Other recent dating studies in Iran show similar ages correlations, as for some incised fan

surfaces in the Sabzevar area (to the north of the study area) dated at 9–13 ka (Fattahi et al. 2006), and for two different generations of Quaternary fans in the Zagros–Makran Transfer Zone (southeast Iran) dated at 5–9 ka and 13.6 ± 1.1 ka by in situ-produced 10Be (Regard et al. 2005, 2006). As a result, given the aforementioned correlations and the studied structures, we can say that if regional aggradation occurred at 53, 25 or 6 kyr and our supposed Quaternary deposits have been faulted after surface abandonment, faulting will be younger than 53 25 or 6 kyr, depending on the age of these faulted Quaternary deposits. Quaternary fracturing with NE–SW trending is clearly attributed to the movements of Kalmard fault zone and the Quaternary tectonic activity of this fault zone in Ozbak-Kuh area is documented in this research (Fig. 14e). Since the effect of faults in Quaternary unit's deformation in the study area is obvious, this deformation can be regarded as another evidence of the tectonic activity which is younger than Mio-Pliocene at Kalmard fault zone. The segments of Kalmard fault zone are the most typical case according to the distribution of Iat. Measurements of the index of relative active tectonics (IAT) classes present that there exists high to moderate amount of deformation in the study area except for the range interior with class 4 (Fig. 5), where the most of geomorphic indices as well as wide valleys (Table 2) and low elevation areas suggest low tectonic activity. This could be related to the inactive folds and faults associated with old deformation. The higher values of Iat with low levels of tectonic activity distribute mainly in the central parts of the study area (basins 22, 29, 32, 35, 61, 70, 71). The lower SL and Hi values, concave hypsometric curves, and higher Vf values in these basins reflect the weak role of tectonic ativity at this part. The combination of the rock strength map (Fig. 2a) with the distributions of computed SL index classes in the area (Fig. 4a) shows that the high and moderate classes mostly correspond to the considerable faults. The anomalous higher SL index in the east and southeastern (basins 62, and 72) and western (basins 53, 74, and 78) parts of the study area were affected by faults F1 and F2 and the rivers which intersect with a high or perpendicular angle. The rock group (resistence) is the same around the anomalous SL which can be interpreted as tectonic signals. Iat is high throughout fault F1 which is the eastern segment of Kalmard fault zone in the Ozbak-Kuh mountains (Fig. 5), which corresponds to structures and morphotectonics landforms in different parts of the study area. The asymmetric factor (Af) clearly shows the tectonic tilting as a consequence of fault movements at the scale of a drainage basin. Due to the tectonic uplift and different movements of the faults, the basins have abnormal SL values, high Hi and so convex hypsometric curves, low Vf values and and Af values. High values of the Hi index generally clear that most part of the uplands have not been eroded, and suggest the younge landscapes which can be created by active tectonics. Some basins in the southeastern part of the study area, such as 8 and 87, which developed above Quaternary alluviums, show high Hi values. Meanwhile, the standard deviations for Hi index values are high (0.078). Furthermore, this impact of the lithology is not enough to explain the variations in the relatively higher or lower Hi values (Chang et al. 2015). The values of Af indicate widespread drainage basin asymmetry related to tectonic processes.

Valley floor widths increase with watershed size, erodibility of rock type, and with decrease of uplift rate. Valley heights decrease with the passage of time after cessation of uplift, but not nearly as fast as valleys widen. In this studty, the values of Vf show that the quick river incision has created narrow valleys as a result of Quaternary tectonic base level fall and tectonic uplift.

The straight or gently curving nature of most faults or folds allows evaluation of the degree of erosional modification of a structural landform. However, erosion dominates landscape evolution after cessation of uplift and creates a sinuous mountain–piedmont junction, especially where lithologic resistance to erosion is weak. Streamflow becomes the dominant process shaping the mountain-front landscape in tectonically quiescent settings. Streams downcut quickly to their base level of erosion by removing small amounts of rock, and then slowly widen their valley fl oors by removing large amounts of detritus derived from hillslopes. The result is a highly sinuous mountain–piedmont junction (Bull 2007). In the study area, tectonic activity along the oblique strike-slip faults have made the linear nature of the fronts. So, the sections of mountain fronts between the subbasins are eroded at slow rate, which have not allowed the embayments to be developed. Smf index commonly is less than 1.1, and maintains the raising mountains along the range-bounding faults.

The knickpoints in the study area are divided into two general categories corresponding to the lithology boundaries and locating on the fault lines. Since most of the faults of the study area are strike slip faults with minor dip slip component, that caused different lithological units with different strengths juxtaposed one another, the knickpoints on the fault lines can not show the current activity of these faults specifically.

The longitudinal river profiles with upward concave shapes show long-term, dynamic equilibrium between uplift and erosion; convex and concave river profiles with knickpoints or knickzones in the middle reaches reflect long-term predominance of erosional processes. However, convex-up rivers profiles are presented in the areas where surface uplift is dominant (Kirby and Whipple 2001).

The results of the longitudinal profiles of the rivers that crossed the fault F1 indicate that this fault has influenced Ksn values so that the rivers show higher amounts where intersect with the fault. At the southwestern part of the fault F1 the high Ksn values can indicate the activity of this fault. The highest Ksn index belongs to the basin 45 with a value of 33.2 (Figs. 7a and 8). The highest values of this indice

correspond with high values of Iat index in different parts of this fault. At all parts of the fault F2 from northeast to southwest, the rivers indicate low to moderate Ksn values in the intersection with this fault (Figs. 7b and 8). Ksn index values through this fault indicate a well correlation with moderate values of Iat index. The Ksn index of the rivers on the fault F3 are medium to high values which belong to middle and southern parts of this fault. Like fault F1, here the Ksn values correspond well with high relative tectonic activity in the study area. The high values of Ksn in the longitudinal profile can confirm the recent activity of this fault (Figs. 7c and 8). Ksn values related to the fault F4 can indicate the activity of this fault. This fault caused increasing of Ksn values on its northeastern and middle parts (basin 62) which represents a well corresponding with high Iat values near Huk village. Ksn values of this fault are nearly medium (basins 77, 73, 62, 33, 51) (Figs. 7d and 9). The Ksn valus through fault F5 are variable so that the highest ones belong to middle and northern parts of it. Based on Iat map, the highest Ksn values correspond with the high values of relative tectonic activity (Figs. 7e and 9). The high Ksn values in southwestern part of fault F6 correspond with high Iat values in southwestern of Gushkamar village (Figs. 7f and 9).

Conclusion

Evaluating morphometric indices have been considered as one of the most important methods through which the relative active tectonics of regions can be assessed effectively. Due to the lack of both seismic record and proper works on active tectonics, we applied this method to the Ozbak-Kuh area in the Kalmard fault zone to identify geomorphic anomalies and evaluate relative tectonic activity, and then corroborated the achieved quantitative results in the field. Since the mean direction of Quaternary fractures is parallel to the general strike of Kalmard fault segments (F1 to F6), it is documented that this fault zone is active in Quaternary. This result is completely correspondent with geomorphic results. There has been the measurement of seven geomorphic indices, such as the stream-gradient index (SL), drainage basin asymmetry (Af), hypsometric integral (Hi), valley floor width–valley height ratio (Vf), drainage basin shape (Bs), mountain-front sinuosity (Smf), and the combination of the above indices (Iat). Based on Iat, we divided the study area into four classes of relative tectonic activities. We found the values of SL, Hi, and Bs to be high along fault F1 (eastern segment of the Kalmard fault zone). The values of Af show high drainage basin asymmetry related to tectonic tilting. The values of Smf suggest that mountain fronts are tectonically active, and the values of Vf show that some valleys are narrow and deep, suggesting a relative high rate of incision. Satellite images, digital elevation models, accurate drainage system data and field observations of the Quaternary structures, the collection of new structural and geomorphic data along the Kalmard fault zone have been used to document a main NE–SW striking, dextral right-lateral brittle deformation zones, which is active in Quaternary. About 80% of the study area has Iat values of classes 1, 2, and 3 indicating moderately to highly active tectonics. Classes 1 and 2 of Iat, indicative of the most active tectonics, occur mainly in the eastern segment of the Kalmard fault zone (fault F1). Class 3 of Iat corresponding to moderately active tectonics, occurs mainly in the western segment of the Kalmard fault zone (fault F2). These classes also correspond well to the areas with young deformed or fractured Quaternary deposits, prominent scarps, triangular facets, deep valleys, and narrow gorges. Furthermore, calculation of normalized steepness index (Ksn) represents significant high values in the eastern and southeastern parts of the study area which correspond well with high values of Iat index. Class 4 of Iat mainly takes place in the center parts of the study area, where all geomorphic indices suggest low tectonic activity. This could be related to structures associated with old deformation in the Ozbak-Kuh area. The dispersal of hypsometric integral, elongation of drainage basins, high anomalies of SL index, and other indices anomalies, represent that the main morphotectonic deformations are a consequence of recent activity. The results of this study imply that the Kalmard fault zone is active in Quaternary.

Acknowledgments The authors appreciate Professor Federico Rossetti and Professor Paolo Ballato of Roma Tre University for their useful comments and precious time to improve our manuscript. Also, we would like to thank Shima Babaei for her great help.

References

Agard P, Omrani J, Jolivet J, Whiterurch H, Vrielynck B, Spakman W, Monie P, Meyer B, Wortel R (2011) Zagros orogeny: a subduction-dominated process. Geol Mag 148:692–725

Alavi M (1991) Tectonic map of the Middle East: Tehran. Geological Survey of Iran, scale 1:5,000,000

Allen M, Jackson J, Walker R (2004) Late Cenozoic reorganization of the Arabia-Eurasia collision and the comparison of short-term and longterm deformation rates. Tectonics 23:TC2008. https://doi.org/10.1029/2003TC001530

Azor A, Keller EA, Yeats RS (2002) Geomorphic indicators of active fold growth: South Mountain–Oak Ridge Ventura basin, Southern California. Geol Soc Am Bull 114:745–753

Bagheri S, Stampli GM (2008) The Anarak, Jandaq and Posht-e–Badam metamorphic complexes in Central Iran: new geological data, relationships and tectonic implications. Tectonophysics 451:123–155

Berberian M, King GCP (1981) Towards a paleogeography and tectonic evolution of Iran. Can J Earth Sci 18:210–265

Berberian M, Mohajer-Ashjai A (1977) SEISMIC RISK MAP OF 1RAN, A PROPOSAL

Bull W.B (1978) Geomorphic Tectonic Classes of the South Front of the San Gabriel Mountains, California. U.S. Geological Survey Contract Report, 14–08-001-G-394, Office of Earthquakes, Volcanoes and Engineering, Menlo Park, CA

Bull WB (2007) Tectonic geomorphology of mountains: a newapproach to paleoseismology. Blackwell, Malden

Bull WB (2009) Tectonically active landscapes. Wiley-Blackwell. https://doi.org/10.1002/9781444312003

Bull WB, McFadden LD (1977) Tectonic geomorphology north and south of the Garlock fault, California. In: Doehring, D.O. (Ed.), Geomorphology in Arid Regions. Proceedings of the Eighth Annual Geomorphology Symposium, State University of New York, Binghamton, pp. 115–138

Calzolari G, Rossetti F, Della Seta M, Nozaem R, Olivetti V, Balestrieri ML, Cosentino D, Faccenna C, Stuart FM, Vignaroli G (2015) Spatio-temporal evolution of intraplate strike-slip faulting: the Neogene–quaternary Kuh-e-Faghan fault, Central Iran. Geol Soc Am Bull 128(3–4):374–396

Calzolari G, Della Seta M, Rossetti F, Nozaem R, Vignaroli G, Cosentino D, Faccenna C (2016) Geomorphic signal of active faulting at the northern edge of Lut block: insights on the kinematic scenario of Central Iran. Tectonics 35(1):76–102

Cannon PJ (1976) Generation of explicit parameters for a quantitative geomorphic study of Mill Creek drainage basin. Oklahoma Geology Notes 36(1):3–16

Chang Z, Sun W, Wang J (2015) Assessment of the relative tectonic activity in the Bailongjiang Basin: insights from DEM-derived geomorphic indices. Environ Earth Sci 74(6):5143–5153

Davoudzadeh M, Soffel H, Schmith K (1981) On the rotation of the Central-East Iran microplate. NeuesJahrbuch für Geologie und Paläontologie (Monatsheft) 3:180–192

Dehbozorgi M, Pourkermani M, Arian M, Matkan AA, Motamedi H, Hosseiniasl A (2010) Quantitative analysis of relative tectonic activity in the Sarvestan area, central Zagros, Iran. Geomorphology 121(3):329–341

El Hamdouni R, Irigaray C, Fernandez T, Chacón J, Keller EA (2008) Assessment of relative active tectonics, southwest border of Sierra Nevada (southern Spain). Geomorphology 96:150–173

Fattahi M, Walker R, Hollingsworth J, Bahroudi A, Nazari H, Talebian M, Armitage S, Stokes S (2006) Holocene slip-rate on the Sabzevar thrust fault, NE Iran, determined using optically stimulated luminescence (OSL). Earth Planet Sci Lett 245:673–684

Fattahi M, Walker RT, Khatib MM, Dolati A, Bahroudi A (2007) Slip-rate estimate and past earthquakes on the Doruneh fault, eastern Iran. Geophys J Int 168:691–709

Flint JJ (1974) Stream gradient as a function of order, magnitude, and discharge. Water Resour Res 10:969–973

Hack JT (1957) Studies of longitudinal streamprofiles in Virginia andMaryland. U.S. Geol Surv Prof Pap 294-B:45–97

Hack JT (1973) Stream-profiles analysis and stream-gradient index. Journal of Research of the US Geological Survey 1:421–429

Haghipour A, Aghanabati A (1989) Geological map of Iran. (2nd edition): Tehran, geological survey of Iran, scale 1:2,500,000

Hare P.W, Gardner T.W (1985) Geomorphic indicators of vertical neotectonism along converging plate margins, Nicoya Peninsula, Costa Rica. In: Morisawa, M., Hack, J.T. (Eds.) Tectonic Geomorphology. Proceedings of the 15th Annual Binghamton Geomorphology Symposium, Allen and Unwin, Boston, pp. 123–134

Hayakawa Y, Matsukura Y (2003) Recession rates of waterfalls in Boso Peninsula, Japan, and a predictive equation. Earth Surf Process Landf 28:675–684

Hayakawa YS, Oguchi T (2009) GIS analysis of fluvial knickzone distribution in Japanese mountain watersheds. Geomorphology 111: 27–37

Jackson J, McKenzie D (1984) Active tectonics of the Alpine—Himalayan Belt between western Turkey and Pakistan. Geophys J Int 77(1):185–264

Kaewmuangmoon S, Thipyopass S, Kosuwan S, Daorerk V, Charusiri P (2008) Investigations on tectonic geomorphology along the Khlong Marui fault, Kao Phanom area, southern Thailand: application of arc GIS approach. In Proceedings of the International Symposia on Geoscience Resources and Environments of Asian Terranes (GREAT 2008), 4th IGCP (Vol. 516, pp. 24–26)

Keller EA (1986) Investigation of active tectonics: use of surficial Earth processes. In: Wallace, R.E. (Ed.), Active tectonics. Studies in Geophysics. National Academy Press, Washington DC, pp. 136–147

Keller E.A, Pinter N (2002) Active tectonics: earthquakes, uplift, and landscape (2ndEd). Prentice Hall, New Jersey

Kirby E, Ouimet W.B (2011) Tectonic geomorphology along the eastern margin of Tibet: insights into the pattern and processes of active deformation adjacent to the Sichuan Basin. In: Gloaguen, R., Ratschbacher, L. (Eds.), Growth and Collaps of the Tibetan Plateau. Geological Society Special Publications, London. 353, pp. 165–188

Kirby E, Whipple K (2001) Quantifying differential rock-uplift rates via stream profile analysis. Geology 29:415–418

Kirby E, Whipple KX, Tang W, Chen Z (2003) Distribution of active rock uplift along the eastern margin of the Tibetan Plateau: inferences from bedrock channel longitudinal profiles. J Geophys Res 108 (B4):2217

Lindenberg HG, Groler K, Jacobshagen V, Ibbeken H (1984) Post-Paleozoic stratigraphy, structure and orogenetic evolution of the southern Sabzevar zone and the Taknar block. NeuesJahrbuch fur Geologie und Palaontologie, Abhhandlungen 168:287–326

Mayer L (1990) Introduction to Quantitative Geomorphology. Prentice Hall, Englewood, Cliffs, NJ

Molin P, Pazzaglia FJ, Dramis F (2004) Geomorphic expression of active tectonics in a rapidly-deforming forearc, sila massif, Calabria, southern Italy. Am J Sci 304:559–589

Mouthereau F, Lacombe O, Vergés J (2012) Building the Zagros collisional orogen: timing, strain distribution and the dynamics of Arabia/Eurasia plate convergence. Tectonophysics 532–535:27–60

Naimi-Ghassabian N, Khatib M-M, Nazari H, Heyhat MR (2015) Present day tectonic regime and stress patterns from the formal inversion of focal mechanism data, in the north of central-East Iran blocks. J Afr Earth Sci 111:113–126. https://doi.org/10.1016/j.jafrearsci.2015.07.018

Nozaem R, Mohajjel M, Rossetti F, Della Seta M, Vignaroli G, Yassaghi A, Salvini F, Eliassi M (2013) Post-Neogene right-lateral strike–slip tectonics at the north-western edge of the Lut Block (Kuh-e–Sarhangi Fault), Central Iran. Tectonophysics. 589:220–233

Pe'rez-Peña JV, Azaño'n JM, Azor A (2009) CalHypso: an ArcGIS extension to calculate hypsometric curves and their statistical moments, applications to drainage basin analysis in SE Spain. Comput Geosci 35(6):1214–1223

Pike RJ, Wilson SE (1971) Elevation–relief ratio, hypsometric integral and geomorphic area–altitude analysis. Geol Soc Am Bull 82:1079–1084

Ramezani J, Tucker R (2003) The Saghand region, Central IRAN: U–Pb geochronology, petrogenesis and implication for Gondwana tectonics. Am J Sci 303:622–665

Ramírez-Herrera MT (1998) Geomorphic assessment of active tectonics in the Acambay Graben, Mexican volcanic belt. Earth Surf Process Landf 23:317–332

Regard V, Bellier O, Thomas JC, Bourles D, Bonnet S, Abbassi MR, Feghhi K (2005) Cumulative right-lateral fault slip rate across the Zagros– Makran transfer zone: role of the Minab–Zendanfault system in accommodating Arabia–Eurasia convergence in southeast Iran. Geophys J Int 162:177–203. https://doi.org/10.1111/j.1365-246X.2005.02558.x

Regard V, Bellier O, Braucher R, Gasse F, Bourlès D, Mercier J, Soleymani S (2006) Be-10 dating of alluvial deposits from southeastern Iran (the Hormoz Strait area). Palaeogeography, Palaeoclimatology, Palaeoecology 242:36–53

Rockwell TK, Keller EA, Johnson DL (1985) Tectonic geomorphology of alluvial fans and mountain fronts near Ventura, California. In:

Morisawa M (ed) Tectonic Geomorphology. Proceedings of the 15th Annual Geomorphology Symposium. Allen and Unwin Publishers, Boston, pp 183–207

Silva PG, Goy JL, Zazo C, Bardajm T (2003) Fault generated mountain fronts in Southeast Spain: geomorphologic assessment of tectonic and earthquake activity. Geomorphology 250:203–226

Stöcklin J (1968) Structural history and tectonics of Iran; a review. Am Assoc Pet Geol Bull 52:1229–1258

Strahler AN (1952) Hypsometric (area–altitude) analysis of erosional topography. Geol Soc Am Bull 63:1117–1142

Takin M (1972) Iranian geology and continental drift in the Middle East. Nature 235:147–150

Troiani F, Della Seta M (2008) The use of the stream length–gradient index in morphotectonic analysis of small catchments: a case study from Central Italy. Geomorphology 102:159–168

Vernant Ph NF, Hatzfeld D, Abassi MR, Vigny C, Masson F, Nankali H, Martinod J, Ashtiani A, Bayer R, Tavakoli F, Chery J (2004) Present day crustal deformation and plate kinematics in the Middle East constrained by GPS measurements in Iran and northern Oman. Geophys J Int 157:381–398

Walker R, Fattahi M (2011) A framework of Holocene and Late Pleistocene environmental change in eastern Iran inferred from the dating of periods of alluvial fan abandonment, river terracing, and lake deposition. Quat Sci Rev 30:1256–1271

Walker R, Khatib M (2006) Active faulting in the Birjand region of NE Iran. Tectonics 25:TC4016. https://doi.org/10.1029/2005TC001871

Whipple KX, DiBiase RA, Crosby BT (2013) Bedrock rivers. In: Schroder J, Wohl E (eds) Treatise on geomorphology, 1824. Academic Press, San Diego, CA, pp 550–573

Wobus C, Whipple K.X, Kirby E, Snyder N, Johnson J, Spyropolou K, Crosby B, Sheehan D (2006) Tectonics from topography: procedures, promise, and pitfalls. Geological Society of America, 398, pp. 55–74